Chapter 1
Facile and Ultrasensitive Sensors Based on Electrospinning-Netting Nanofibers/Nets

Yan Li, Jianyong Yu, and Bin Ding

Abstract Due to rapid growth of industrialization, urbanization and modern agricultural development, there has resulted a heavy backlog of gaseous and liquid pollution in all over the world and threated the health of human beings. Driven by the actual demand, the sensors possess good portability, easy usability, excellent selectivity and sensitivity for water and air pollution monitoring are highly desirable. Among versatile sensing platforms, quartz crystal microbalance sensors and colorimetric sensor gained increasing attention for their easy accessibility, favorable expansibility and good associativity. Based on above two platforms, nanofibrous materials have been choose as an idea substrate to either capture the marker or amplify the signal associated with detection. In this chapter, we reviewed recent progress in the development of electrospun nanofibrous materials having applications in two predominant sensing approaches (quartz crystal microbalance and colorimetric sensors), illustrate them with current examples showing how they have been applied, optimized and discuss their intrinsic fundamentals and optimal designs. Moreover, we will also highlight gaps requiring further research.

1.1 Introduction

Due to rapid growth of industrialization, urbanization and modern agricultural development [1–4], there has resulted a heavy backlog of gaseous and liquid pollution in all over the world, which include inorganic gases (NH_3, CO_2, SiO_2,

Y. Li
Key Laboratory of Textile Science & Technology, Ministry of Education, College of Textiles, Donghua University, Shanghai 201620, China

J. Yu
Nanomaterials Research Center, Modern Textile Institute, Donghua University, Shanghai 200051, China

B. Ding (✉)
Key Laboratory of Textile Science & Technology, Ministry of Education, College of Textiles, Donghua University, Shanghai 201620, China

Nanomaterials Research Center, Modern Textile Institute, Donghua University, Shanghai 200051, China
e-mail: binding@dhu.edu.cn

A. Macagnano et al. (eds.), *Electrospinning for High Performance Sensors*, NanoScience and Technology, DOI 10.1007/978-3-319-14406-1_1

$N(CH_3)_3$, etc.) [5–7], volatile and semi-volatile organic hydrocarbons, aldehydes, and heavy metals (Hg(II), Pb(II), Cu(II), Cr(IV), etc.) [8–10]. As is known to all, the air we breathe and the water we drink are essential ingredients for our wellbeing and a healthy life [11, 12]. Unfortunately, we are all routinely exposed to a broad range of pollutants that are present within the environment. Over the last three decades there has been increasing global concern over the public health impacts attributed to environmental pollution, in particular, the global burden of disease [13–16]. As the World Health Organization (WHO) stated, one sixth of the world's population, approximately 1.1 billion people do not have access to safe water and 2.4 billion lack basic sanitation [17]. Especially some trace heavy metals in polluted water are seriously harmful to human health [9]. On the other hand, in a recent study, WHO reports that in 2012 around seven million people died – one in eight of total global deaths – as a result of air pollution exposure. This finding more than doubles previous estimates and confirms that air pollution is now the world's largest single environmental health risk [18, 19]. Consequently, rapid detection of contaminants in the environment by emerging technologies is of paramount significance [5, 12, 20]. A tool providing interactive qualitative and quantitative information about pollution is essential for policy makers to protect massive populations.

Driven by the actual demand, various equipment have been built up for the quantification of water and air pollution in the past decade, such as inductively coupled plasma mass spectrometry [21, 22], atomic absorption spectrometry [23, 24], anodic stripping voltammetry [25, 26], and high performance liquid chromatography [27]. Although these strategies provide accurate, ultrasensitive detection, most of them require tedious sample pretreatment before analysis, and generally are not amenable to be handled by unskilled personnel. Therefore, it is highly desirable to develop a portable, easy use, selective and sensitive method for water and air pollution monitoring. Compared with those sophisticated equipment, quartz crystal microbalance sensors and colorimetric sensors gained increasing attention for their easy-to-use, relatively low cost and no requirement for skillful technicians [28, 29]. Until now, considerable efforts have been devoted to the assay of hazard gases and polluted water based on above two platforms. However, the sensitivity of those previously reported QCM and colorimetric sensors are still not sufficient magnitude to allow for practical applications [30–33].

In parallel, as one kind of the most important nanomaterials, electrospun nanofibrous materials have gained an increasing of interest in the environmental applications because of their unique chemical and physical properties, for instance, small size, large specific surface area (SSA), three dimensional (3D) porous structure, amenable to surface modification, etc. [34–36]. Under this circumstance, nanofibrous materials are used to either capture the marker or amplify the signal associated with detection [35]. Both of these capabilities are important for trace level pollution detection which are also hardly realized by utilizing conventional materials. Benefiting these unique properties, nanofibrous materials based sensors have be applied to assay, degrade and scavenge pollutants in water and air in the past decades [37–39].

In this chapter, we will review recent progress in the development of electrospun nanofibrous materials having applications in two predominant sensing schemes (QCM and colorimetric sensors), illustrate them with current examples showing

how they have been applied and optimized. Moreover, we will also discuss their intrinsic fundamentals and optimal designs. Ultimately, we will also highlight gaps requiring further research.

1.2 Electrospinning and Electro-Spinning/Netting (ESN)

1.2.1 Electrospinning

Amongst number of processing techniques have been used to prepare polymer nanofibers, electrospinning is currently the most effective technique that allows the fabrication of continuous fibers with diameters down to a few nanometers, which shares characteristics of both electrospraying and conventional solution dry spinning [40].

1.2.1.1 The Process of Electrospinning

Electrospinning, also known as electrostatic spinning, is a powerful, rather simple and highly versatile technique which allows fabricating micro-and nanoscale fibers from process solutions or melts using and electrically forced fluid jet [41]. A schematic diagram to interpret electrospinning of polymer nanofibers in shown in Fig. 1.1. During the electrospinning, a high voltage electric field, is applied to the polymer liquid (a solution or melt), the repulsion among the charges on the surface of the drop at capillary tip competes with the surface tension, which tends to stabilize the drop [42, 43]. Once a critical condition is reached at which surface charge repulsion dominates, the hemispherical surface of the liquid at the tip elongates to form a conical shape known as the Taylor cone [44, 45]. Further increasing the intensity of the electric field, a jet is drawn from the spinneret under a constant flow rate. Before reaching the collector, the solution jet evaporates or solidifies, and is collected as an interconnected mats of small fibers on the oppositely charged grounded collector [46]. The diameters of polymer fibers are around nanometers, from few tens nanometers to micrometers, a typical example of polyacrylonitrile (PAN) nanofibers is displayed in Fig. 1.1.

1.2.1.2 Rich and Varied Electrospun Nanofibers

As a nanofabrication technique, electrospinning has been identified as a remarkably robust and versatile method for fabricating fibers with diameters down to the nanometer length scale by applying a high voltage on a polymer solution or melt. A variety of materials such as polymers [47–50], ceramics [51–53], carbon [54–56] and even metals [57] have been electrospun into uniform fibers with well-controlled

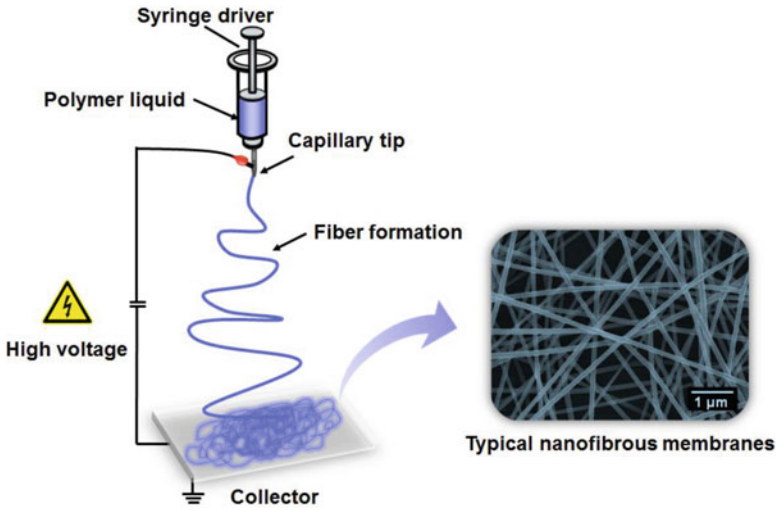

Fig. 1.1 Schematic diagram of fundamental setup for electrospinning

sizes, compositions, and morphologies. In most occasion, electrospun nanofibers are usually smooth solid fibers and they are collected as nonwoven membranes with randomly arranged structures, which have great limited their applications in various areas, for instance, electronic devices, biomedical areas, etc. [58] Thus it is important to have a basic understanding of the different group of materials and versatile nanofibrous structures before selecting the most appropriate electrospun fibers for sensing application. In order to fully explore the application of nanofibers, more and more scientists try to fabricate nanofibers with rich and varied structures. Different nanofiber structures and morphologies can be obtained *via* control of the processing conditions, these structure regulations could be mainly divided into two categories: single fiber structure and aggregate structure.

The single fiber structure is of significant importance as far as the packing of the fibers is concerned in nonwovens-that is, the total porosity. Furthermore, the structure is of significance with respect to the internal specific surface as controlled by geometric effects, but also with respect to the shape of the pores controlled by intersecting fibers as well as with respect to the flow of fluids or gases around the fibers that is, the permeation properties [40, 59]. So far, by regulating different parameters include the solution properties such as viscosity, elasticity, conductivity, and surface tension; governing variables such as hydrostatic pressure in capillary tube, electric potential at the capillary tip, and the distance between the tip and the collector; and the ambient parameters such as solution temperature, humidity, and air velocity in the electrospinning chamber, the nanofibers with porous [60], ribbon-like [61], helical [62], necklace-like [63], pine-needle-like [64], firecracker shape [65], multi-channel tubular [66], nanowire-in-microtube [67, 68] are successfully fabricated, as shown in the Fig. 1.2.

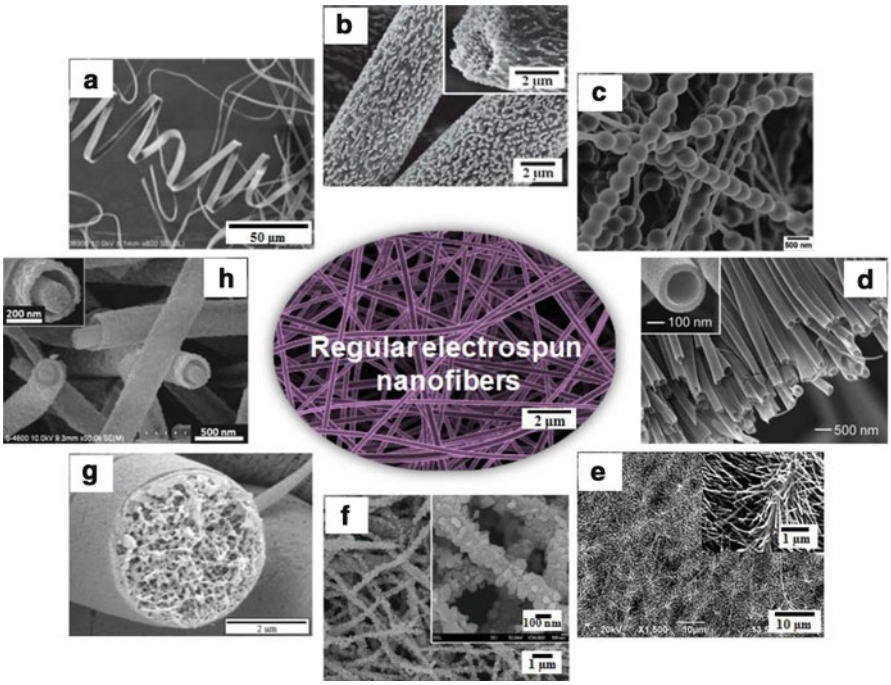

Fig. 1.2 Various micro-and single nanofibrous structures fabricated by electrospinning. (**a**) ribbon-like, reprinted with permission from [61]. ©2014 American Chemical Society; (**b**) porous, reprinted with permission from [69]. ©2012 Royal Society of Chemical; (**c**) necklace-like, reprinted with permission from [55]. ©2012 American Chemical Society; (**d**) hollow, reprinted with permission from [70] ©2004 American Chemical Society; (**e**) pine-needle-like, reprinted with permission from [64]. ©2012 Elsevier Ltd.; (**f**) firecracker-shaped, reprinted with permission from [68]. ©2014 Royal Society of Chemical; (**g**) inner porous, reprinted with permission from [71]. ©2010 American Chemical Society; (**h**) wire-in-tube structures, reprinted with permission from [68]. ©2010 American Chemical Society

Besides controllable fabricating versatile of single fiber structure, many groups have demonstrated that electrospun nanofibers could be collected as uniaxial aligned arrays since the collection of fibers aligned along a preferential direction is a very relevant aspect to be considered for various applications [72, 73]. For instance, Ding et al. use the high speed rotating roller as collecting electrodes, the strong stretching of the roller makes the fiber to be aligned among the rotating orientation, the highly alignment Poly(m-phenylene isophthalamide) (PMIA) nanofibers have been successfully fabricated, as shown in the Fig. 1.3a. Here is another typical example, Li et al. reported that nanofibers could be uniaxially aligned by introducing insulating gas into conductive collectors [74]. The more complex aggregate structure of nanofibers such as hierarchically organized nanofiber composites could also realize. To electrospun nanofiber membranes, lack of structural integrity is a persist problem and restrict its commercial viability.

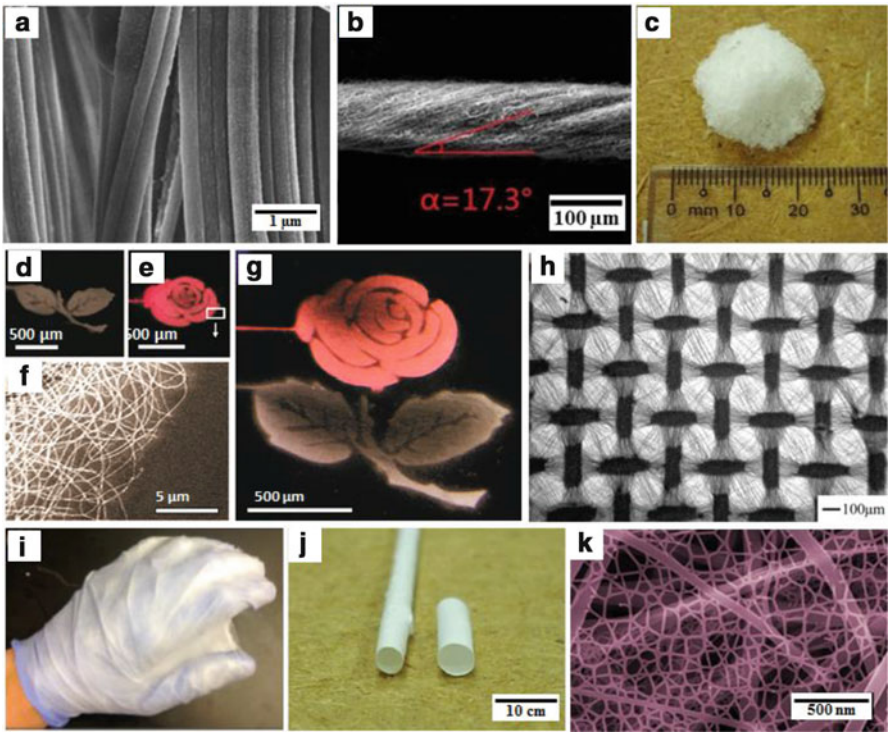

Fig. 1.3 Different aggregate structure of electrospun nanofiber: (**a**) alignment nanofiber, (**b**) yarns, reprinted with permission from [81], ©2013 Springer Science + Business Media; (**c**) 3D assemblies, (**d–h**) patterning nanofibers, (d–g) reprinted with permission from [75]. ©2010 American Chemical Society; (**h**) reprinted with permission from [76]. © 2007 WILEY-VCH Verlag GmbH & Co.; (**i**) glove sharp nanofibers, reprinted with permission from [76]. ©2014 American Chemical Society; (**j**) tubular nanofibers structure, reprinted with permission from [82]. © 2011 IOP Publishing Ltd.; (**k**) 2D nanonets, reprinted with permission from [83]. © 2011 Royal Society of Chemistry

Hierarchically organized nanofiber composites have great potential to solve this problem because they allow for interfacing nanofibers with other structural surfaces, and therefore the advantages of both components can be utilized synergistically. For example, as shown in Fig. 1.3d–g, Cho et al demonstrated selectively deposited architectures, well aligned fibrous architectures, and multilayered architectures [75]. Zhang et al fabricated the uniform mesh-like PLLA patterning nanofibers by using electroconductive collector with woven structure, which is displayed in Fig. 1.3h [76]. Furthermore, there are numerous hierarchically organized nanofiber composites, such as yarns, multiple interconnecting tubes, glove shaped, 3D assemblies, etc. [77–80] It has been shown that the outstanding properties and multifunctionality of such nanofibers and nanofibrous aggregates are highly attractive to numerous applications, including biological engineering,

composite, filters, textiles, etc. Additionally, this technique has become particularly powerful when combining other remarkable features with unique chemical, physical, and mechanical functions provided by adding other components with ease and control. Last but not least, electrospinning opens a door to creating various micro- or nanostructures for sensing application.

Notwithstanding the ability to fabricate micro- and nanoscale fibers of electrospinning which provide great potential in different fields, it is still difficult to electrospun polymer into uniform nanofibers with diameter as several nanometers up to now [84]. On the other hand, enormous researches in the past 10 year have indicated that the large average diameter (100–500 nm) of common electrospun fibers blocked their further applications in ultrafiltration, ultrasensitive sensors, catalyst, etc. In a meantime, when the fiber diameter falls below 20 nm [85], the extra SSA and porosity become more significant. Therefore, developing a robust strategy for manufacturing large-scale and extremely small nanofibers (<50 nm) has been a hotspot in the field of nanotechnology. As shown in Fig. 1.3k, a 2D soap bubble-like structured nanonets are fabricated for the first time by Ding et al in which the primary electrospun fibers acted as a support for the nanonets comprising interlinked ultrathin nanowires with diameter of 5–40 nm. This new types of aggregate structure was termed as "electrospun nanofibers/nets (NFN) membranes" was obtained by employing the novel one-step "electro-spinning/netting (ESN)" process which will be detailed introduced in the following part [86]. This inimitable structure exhibits several amazing characteristics, such as an extremely large SSA, high porosity and superior mechanical performance.

1.2.2 ESN Technique

In the past few years, significant progresses have been made in term of our fundamental understanding of the ESN process, the controllable fabrication of NFN membranes based on different polymer systems also have been explored. ESN NFN membranes has undoubtedly risen as a shining star in the horizon on the path of the scientists' searching for new materials for future environment, energy and healthcare applications [87]. Benefitting several fundamental properties of itself, such as extremely small diameter, high porosity, Steiner tree network geometry, controllable coverage rate, and controllable density, there is no doubt that NFN membrane are also an attractive candidate as sensing substrate loaded with receptors for ultrasensitive sensors. The following sections will fully illustrate the strategies for the controllable fabrication of NFN membranes.

1.2.2.1 History of ESN

The origins of the NSN process can be traced to the year of 2006 through a research article published in the journal of "*Nanotechnology*" by Ding and coworkers. An

incompletely spited polyacrylic acid (PAA) spider-web-like or soap-bubble-like structure were observed, then such unexpected unique structure was officially named as "nanonets" on account of its fascinating features [87]. In the meantime, the principles of structure control and a possible formation mechanism was also preliminary studied. It is at this time, the concept of "ESN" was introduced. As a variant of electrospinning process, ESN process involves the use of a high voltage to induce the formation of a liquid jet. In addition to the formation of liquid jet, the ESN process also comprise an electro-netting process, which defined as the phase separation-induced splitting of a small charged droplet in a high electric field. Since then, the research on exploration of spinnable polymers, influencing parameter, morphology control, application optimize has grown exponentially.

1.2.2.2 Formation Mechanism of NFN Membrane

About 8 years after the fantastic ESN was demonstrated by Ding, a wealth of researchers continued to expand the suitable application areas of NFN membranes and fell over themselves to learn as much as they could understanding the formation mechanism of NFN membrane on the other side. The questions keep arising during the research process, such as where is this structure come from? What happens to the charged polymer jets and droplet during their running in such small distance between the capillary tip and grounded collector? All these questions have triggered more rigorous experimental and theoretical work to reveal the secrets behind ESN process [72]. We are very delighted to hear and see that more and more researchers devoted themselves in this domain, but it is also worth to point out that the formation mechanism of NFN structures is complex and consensus on the formation mechanism has not been reached.

Up till the present moment, there are four predominant mechanism to explain the formation of NFN membrane which include the "ions initiated splitting up of the electrospun fibers" that proposed by Kim et al [88]. According their recent work, the nanonets are formed by the joints between many fibers and the possible joints occur at the apex of Taylor cone. In addition of "ions initiated splitting up of the electrospun fibers", Kim and his coworkers have proposed the "hydrogen bond formation" between nano-nets and PA6 nanofiber scaffold based on the investigation of PA6 and methoxy poly (ethylene glycol) (MPEG) oligomer/PA-6 NFN membranes [89, 90]. Another plausible mechanism of nanonets is "intertwine among branching jets", which is put forward by Tsou et al. base on their theoretic, the formation of nano-nets is associated with the complicated interaction between the subsidiary jets [91]. The last one is a mechanization proposed by Ding et al. That is "phase separation of charged droplets" theoretic which also has been well known and we will emphatically introduces next [92].

Since Ding et al observed the defect PAA films and partly split PAA nano-nets during 2006, they proposed the mechanism of "phase separation of charged droplets" for the first time depended on those observation described above. According to

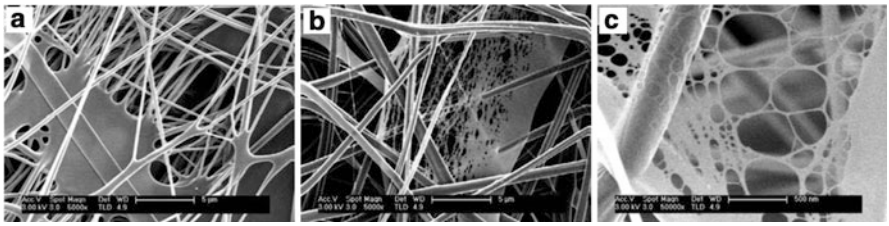

Fig. 1.4 SEM images of PAA fibers formed in PAA solution combined with (**a**) H_2O and (**b**) ethanol at a concentration of 6 wt%, voltage of 30 kV, spinning distance of 15 cm and relative humidity of 20 %. (**c**) High magnification SEM image taken from the sample shown in (**b**) (Reprinted with permission from [92]. © 2006 IOP Publishing Ltd)

the mechanism, the formation of nano-nets is on account of the phase separation of charged droplets generated during electrospinning. They suggested that during the ESN process, in addition to the formation of polymer solution jet, it also splitted some small charged droplets in a high electric field [93]. The discharged polymer solution jet undergoes an instability and elongation process, which allows the jet to become very long and thin and eventually form the polymer nanofibers. For small charged droplet, it deforms significantly to a thin liquid film, which undergoes rapid phase separation with the solvent rich domains to transform into pores. Actually, the presumption of small charged droplets formation is not an idiosyncratic views. The break-up of a jet and the formation of small charged droplets is a very old and interesting problem and the relevant research can be trace back to last century. For instance, in 2000, Hartman et al. presented a physical numerical model to describe the harmonic perturbations on the jet surface based on a cylindrical coordinate system, thereby to model the jet break-up process with analytical relations [94] (Fig. 1.4).

A schematic diagram illustrating the possible formation procedure of nano-nets is shown in Fig. 1.5. After the microsized charged droplets generated accompanying with the electrospun jet, There are various forces act on the charged droplet when it flights with a high speed in the electric field, including electrostatic force, drag force, gravity, Coulombic repulsion force, surface tension and viscoelastic force [95–97]. Above forces all play an important roles during the process of nano-nets formation. The electrostatic force is response to carry the charged droplet from capillary tip to collector. The drag force between the surrounding air and the charged droplet is the main cause that deforms the droplets into films. As to the Coulombic repulsion force, the main function is keep expanding the droplet. In addition, the contraction of charged droplet is attributed to the surface tension and viscoelastic forces. Since the electric field could be increased by increasing the applied voltage within a constant distance, the electrostatic and Coulombic repulsion forces of charged droplet were reinforced with increasing of electric field consequently. Then, the moving of charged droplet is further accelerated due to the increased electrostatic force, which led to an increased drag force. This

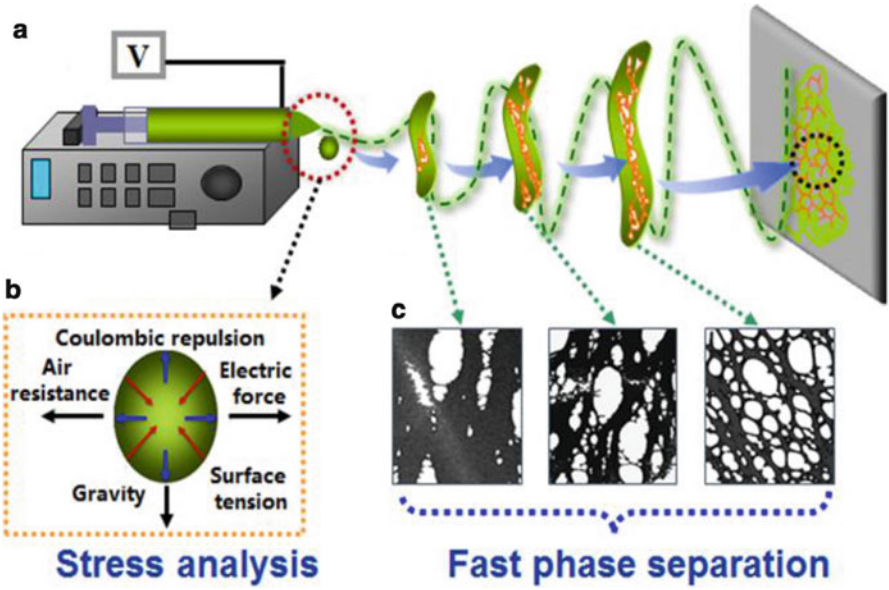

Fig. 1.5 (**a**) Schematic diagram of setup of electro-spinning/netting apparatus, reprinted with permission from [98]. © 2011 Royal Society of Chemistry. (**b–c**) Show drawings of the forces acting on the charged droplet and the possible process of nano-nets formation during ESN process (Reprinted with permission from [92]. © 2006 IOP Publishing Ltd)

phenomenon of charged droplet distortion and expansion in the electric field was also reported by Grimm and Beauchamp during their research on electrospraying [95]. The further expansion could happen when the electric field increased further to form thin films from droplets with the effect of increased Coulombic repulsion and drag forces. Moreover, the increased radial charge repulsion force also has a tendency to expand the charged films. As a result, the deformation of charged droplet was strongly affected by the electric field.

1.2.2.3 NFN Membrane Based on Different Polymer Systems

As introduced above, much effort has been applied to NFN membranes to comprehend the fundamental phenomena of fabrication process as well as the physical and chemical properties from the material science viewpoint. Consequently, ESN has been applied to numerous kind of polymer systems, including polymers soluble and spinnable from water, biocompatible and biodegradable polymers, polymer blends and polymers into which nanoparticles, salts, surfactants and other functional materials have been incorporated. Here is a comprehensive summary of polymers that have been successfully ESN into NFN structures to-date (Table 1.1).

Table 1.1 Different polymers to have been ESN into NFN membranes

Polymer system	Molecular weight	Solvent	Applications	Ref.
PA-6	18,000	Formic acid	Filter; sensors	[83, 99, 100]
PA-66	15,000	Formic acid	Filter	[101]
PAA	250,000	H_2O/Formic acid/ Ethanol	Sensors	[92, 97, 102]
PVA	90,000	H_2O	Filter; sensors	[88]
PU	180,000	DMF, DMF/THF	Filter; protective clothing; tissue engineering	[96]
CS	210 KDa	Acetic acid/H_2O	Tissue engineering; wound healing	[103]
Gelatin	–	Formic acid/ acetic acid	Tissue engineering; wound healing	[104]
PAA/PA-6	–	Formic acid	Sensors	[105]
CS/PA-6	–	Formic acid	Tissue engineering	[106, 107]
PANI/PA-6	–	Formic acid	Sensors	[108]
PANI/PVB/ PA-6	–	Formic acid	Sensors	[109]
NC/PA-6	–	Formic acid	Sensors	[110]

PA-6 polyamide-6, *PA-66* polyamide-66, *PVA* polyvinyl alcohol, *PU* polyurethane, *CS* chitosan, *PANI* polyaniline, *PVB* polyvinylbutyral, *NC* nitrocellulose, *DMF N,N*-dimethylformamide, *THF* Tetrahydrofuran

As shown in the Fig. 1.6, the typical morphologies of NFN membranes based on different polymer systems, such as PAA, PA-6, PMIA, gelatin, CS, and PU, which have been synthesized in Ding's laboratory. By regulating the different polymer systems and optimizing the nano-nets morphology (e.g. fiber and nanowire diameter, pore-width and coverage rate of nano-nets), they have found out that similar to electrospinning, the ESN process is also influenced by many parameters, classified broadly into solution parameters, process parameters, and ambient parameters. Solution parameters include concentration, conductivity, viscosity, surface tension, and solvent all influence the phase separation process during the ESN [86, 96, 98, 99]. As to process parameters, which include applied voltage and tip to collector distance. Each of these parameters significantly affects the NFN morphology. Except these influence factors, ambient parameters enclose the temperature and humidity of the surroundings, which also play a significant role in determining the morphology of NFN membranes. Although we already have a general knowledge of formation mechanism and influence factors of NFN membranes as well as successfully fabricated a broad range of polymers into NFN membranes, it is worth pointing out that the relationship lie behind appearances between spinnable polymers and NFN membranes is still waiting us to reveal.

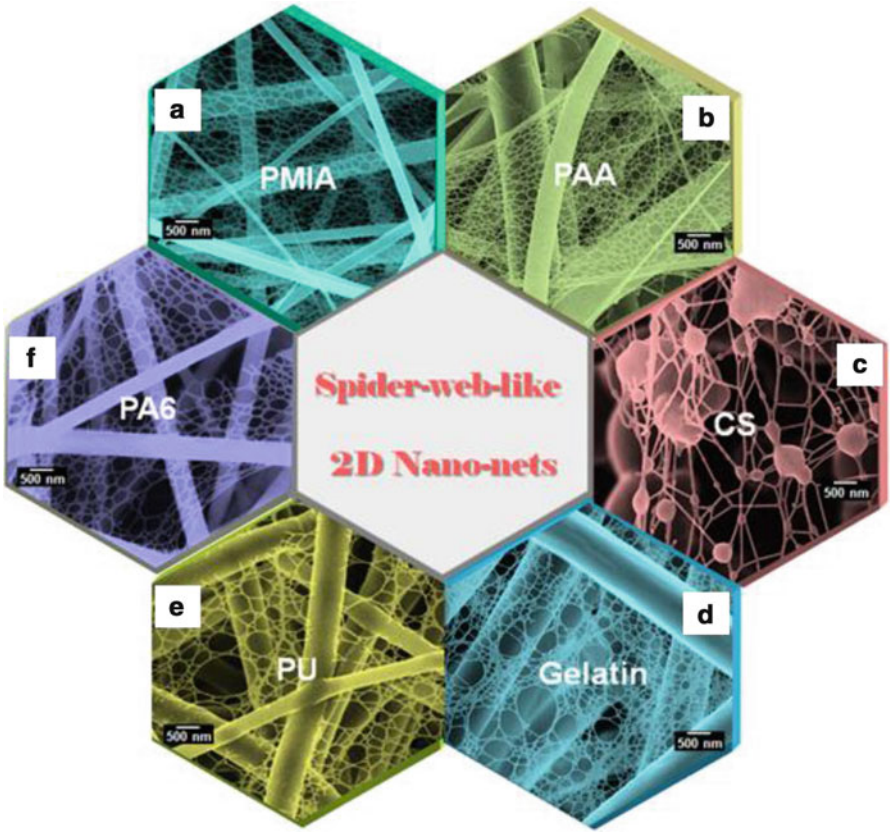

Fig. 1.6 Several typical electrospun nano-fibers/nets membranes based on different polymer systems. (**a**) PMIA; (**b**) PAA; (**c**) CS; (**d**) gelatin, reprinted with permission from [104]. © 2011 Elsevier Ltd.; (**e**) PU, reprinted with permission from [96]. © 2011 WILEY-VCH Verlag GmbH & Co.; (**f**) PA6

1.3 Sensors Based on Electrospun Nanofibers and ESN NFN Membranes

In recent years, considerable efforts have been made to develop varied sensors for the assay of environmental contaminants. Benefiting from the large surface-area-to-volume ratio, tailored pore structures, large stacking density and ease to surface modification of electrospun nanofibrous membranes, the nanofiber and NFN membranes-based sensors achieve high sensitivity, fast response, and good reversibility. In this section, we will review recent progress in the development of electrospun and ESN materials based QCM and colorimetric sensors, illustrate them with current examples showing how they have been applied, and discuss their intrinsic fundamentals and optimal designs.

1.3.1 QCM Sensors

In 1959, Sauerbrey demonstrated the dependence of quartz oscillation frequency on the change in surface mass [111]. He coined the term QCM in late 1950s, and it was his work that led to the use of quartz plate resonators as sensitive microbalances for thin films. When voltage is applied to a quartz crystal causing it to oscillate at a specific frequency, the change in mass on the quartz surface is directly related to the change in frequency of the oscillating crystal, the mass-frequency shift relation for quartz crystal resonators as follows [112, 113]:

$$\Delta f = -2f_0^2 \Delta m / A(\mu\rho)^{1/2} \tag{1.1}$$

Where Δf the measured frequency shift, f_0 fundamental frequency of a bare QCM chip, Δm the mass change per unit area, A the electrode area, ρ the density of quartz, and μ the shear modulus of quartz crystal.

For QCM, the most unique feature is the change in frequency can determine the mass of analyte adsorbed in ng/cm^2. Consequently, enormous materials such as metals, ceramics, polymers, self-assembled monolayers, lipids, and waxes, have been used as sensitive coatings on QCM to improve the sensor sensitivity and selectivity for chemical analytes [114, 115]. One major challenge lies in that the flat electrode surface limits the immobilization degree of the absorbing sites per unit area accompanies with the rapid development of QCM sensors [116]. Driven by the actual need, increasing attention has been paid to the development of nanostructured coatings on QCM to improve the sensor sensitivity, for instance, nanofibers [117]. Taking advantage of large specific surface area of the nanostructured sensing materials, the performance of the QCM sensors is greatly enhanced. In this part, we review recent progress in the development of electrospun and ESN nanomaterials having applications in QCM sensing approaches.

Formaldehyde is one of the volatile organic compounds (VOCs) that are widely used in household materials, which is associated with many health risk factors and has been identified as a major cause of sick building syndrome [118–120]. Consequently, the WHO has set a 30 min exposure limit of 0.08 ppm, while the US National Institute for Occupational Safety and Health has established a maximum long-term exposure limit of 0.016 ppm [121]. Considering the harmfulness of formaldehyde, the fast, selective and sensitive detection seems extremely important. Polyethyleneimine (PEI), a cationic polyelectrolyte, has been investigated not only as an immobilization material for biosensors, but also as a sensing materials for various gases and vapors. PEI has an affinity with formaldehyde, resulting from the interaction between formaldehyde molecules and amine groups of PEI [122]. Therefore, we are going to introduce a series of QCM formaldehyde sensor utilizing the PEI as the sensing material.

1.3.1.1 PEI Functionalized Polystyrene (PEI@PS) Nanofibrous Membranes Based Formaldehyde Sensors

SSA as a vital factors of QCM surface which determines the immobilization degree of the absorbing sites per unit area, thereby plays a decisive role in sensitivity. Since developing materials with a porous structure is an accepted way to enhance the available surface area, Zhang et al. [117] fabricated a formaldehyde sensors by depositing the three-dimensional (3D) fibrous PS membranes with different porous structure on the QCM surface (Fig. 1.7a). Then modified PEI solutions onto fibrous PS membranes, through which fibrous PEI@PS membranes were obtained. The resultant composite membranes were investigated as sensitive coatings on QCM for formaldehyde detection at room temperature. As shown in Fig. 1.7b, BET surface area test and N_2 adsorption/desorption isotherm demonstrated that PS fibers electrospun from higher concentration of PS solution (13 wt%) tended to possess larger pore volume and SSA (42.25 m^2/g), offering an excellent sensing template for the modification of PEI. In this case, when exposed to 140 ppm of formaldehyde, QCM-based PEI@PS (13 wt%) sensors has achieved the largest response value, approximately four times as much as PEI@PS (7 wt%) sensors. As it displayed in Fig. 1.7c, the developed formaldehyde-selective sensors exhibited fast response and achieved a detection limit of 3 ppm at room temperature.

In order to further improve the sensitivity of PEI@PS based sensors, Zhang et al subsequently investigated the influence of PEI depositing quantity, as shown in Fig. 1.7d, when exposed to 140 ppm of formaldehyde, the maximum frequency shifts of the PEI@PS based QCM sensors with various PEI coating loads (1,000, 2,000, and 6,000 Hz) were 5, 33, and 75 Hz, respectively. It was observed that the response of the sensor coated with 6,000 Hz PEI was almost 15 times as much as that of the sensor coated with 1,000 Hz PEI. As expected, the detecting sensitivity increased with the amount of PEI deposited on the QCM electrode due to more absorbing sites. Unfortunately, the optimal quantity of PEI to achieve the best performance of formaldehyde is not obtained here, because the QCM system would overload when the coating load of PEI is above 6,000 Hz. Additionally, from the Fig. 1.7e we can know that the developed sensors perform excellent selectivity toward formaldehyde when exposed to other interfering VOCs.

1.3.1.2 PEI Functionalized Titanium Dioxide (PEI@TiO2) Nanofibrous Membranes Based Formaldehyde Sensors

On the consideration of semiconductor metal oxides fibrous materials' advances in facilitating rapid mass transfer of the analyte molecules to and from the interaction region and requiring charge carriers to traverse any barriers introduced by molecular recognition events along the entire fibers [123, 124]. Wang et al. [120] developed another nanostructured complex of PEI functionalized TiO_2 nanofiber (PEI@TiO_2) as sensing coating on QCM for formaldehyde detection. As shown

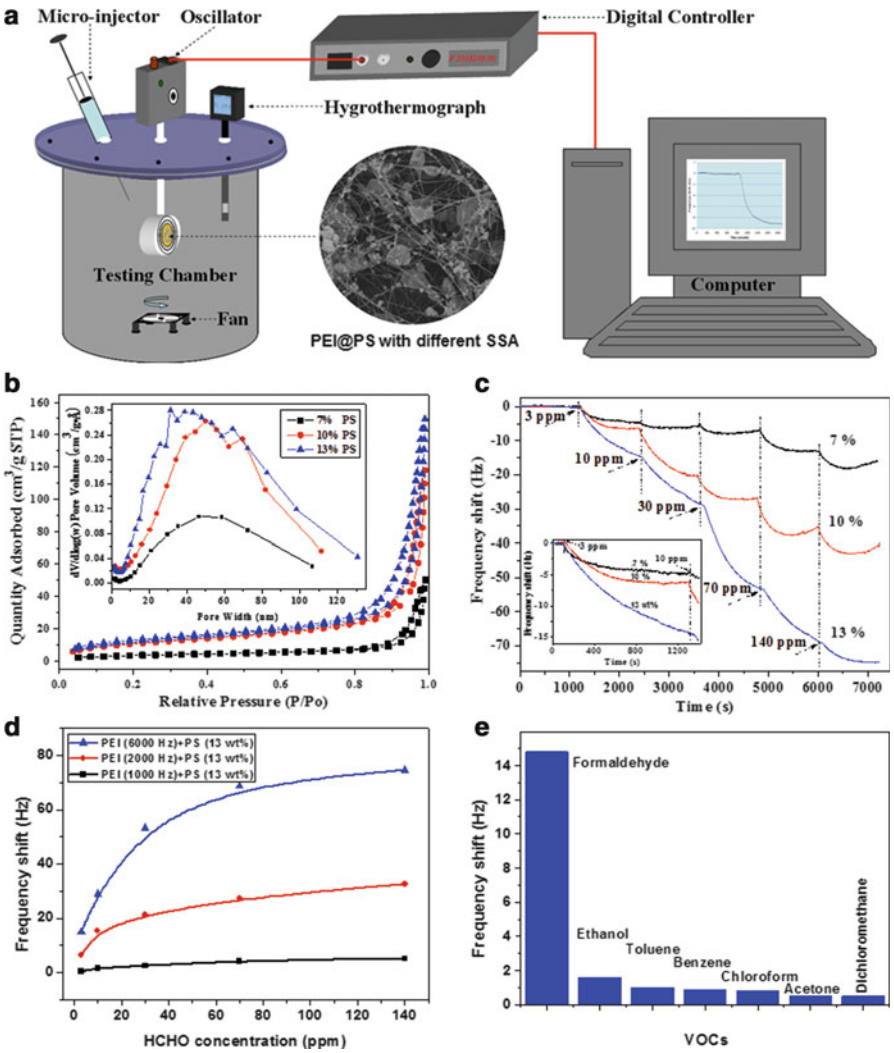

Fig. 1.7 Schematic diagram of a gas testing system based on PEI@PS with different SSA for formaldehyde monitoring (**a**). Nitrogen adsorption and desorption isotherm of fibrous PS membranes with different concentration, the inset image shows the pore size distribution (**b**). Response of QCM-based PEI-PS sensors formed from various concentrations of PS solutions (**c**). The influence of PEI loading amount (**d**), and the frequency shift of QCM-based PEI@PS sensors versus 30 ppm of various VOCs (**e**) (Reprinted with permission from [117]. © 2011 Elsevier Ltd)

in Fig. 1.8, the 3D porous TiO_2 fibrous membranes with porous structure were successfully fabricated by calcining the TiO_2/PS fibers at 450 °C. The porous structure of TiO_2 fibers was also confirmed by the nitrogen adsorption–desorption isotherm, the nitrogen adsorption–desorption isotherm of the TiO_2 fibers exhibits a type IV adsorption branch with a combination of H1 and H3 hysteresis loops

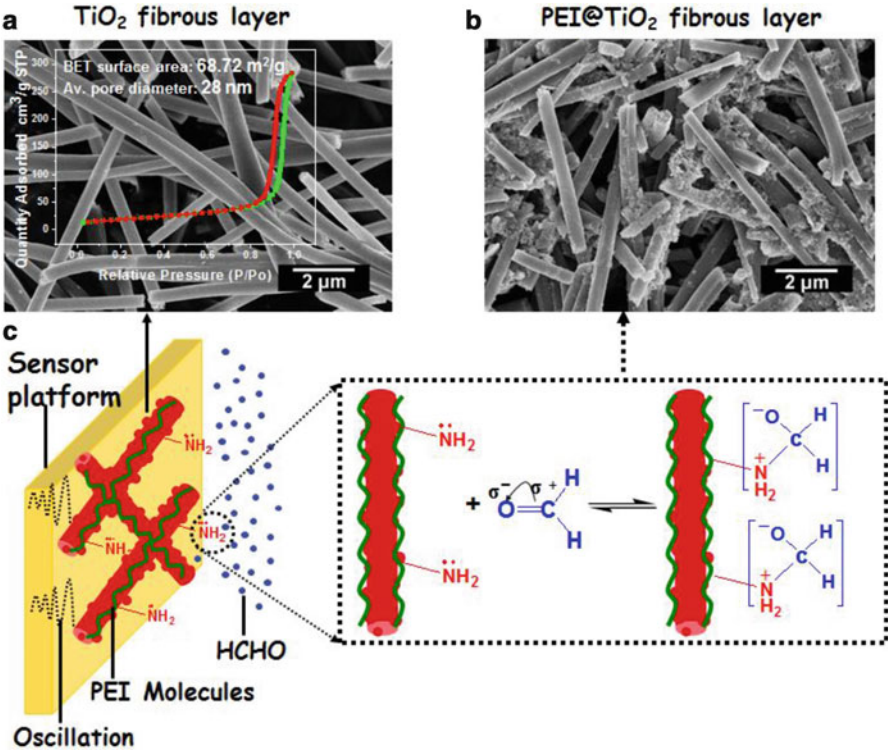

Fig. 1.8 The typical FE-SEM images of TiO_2 (**a**) and PEI@TiO_2 nanofibrous membranes (**b**), the inset image of (**a**) shows the nitrogen adsorption and desorption isotherm of TiO_2 membranes. And the (**c**) schematic represents the detecting platform of formaldehyde vapor based on PEI@TiO_2 fibers (Reprinted with permission from [120]. © 2012 Elsevier Ltd)

characteristic of a predominantly mesoporous system [125, 126]. The calculated BET surface area and average pore diameter are 68.72 m^2/g and 28 nm, respectively. All these versatile structures make the TiO_2 to be a candidate for applications of formaldehyde sensing.

The formaldehyde-sensing properties of PEI@TiO_2 porous fibers on QCM were investigated by measuring the frequency changes when the fibers were exposed to formaldehyde vapors. During the exposure process, the porous fibers on the QCM act as sensing layers for target formaldehyde molecules and the interaction of formaldehyde molecules with the sensing layer causes the frequency to decrease. The sensor responses (ΔF) for each concentration were obtained from the frequency differences between the corresponding QCM frequencies at the beginning and the end of the exposure process. Figure 1.9a shows time courses of response of PEI@TiO_2 sensors with different PEI coating loads upon exposure to increasing formaldehyde concentrations (1–100 ppm) in a cell. The QCM sensor coated with only TiO_2 fibers exhibited only 0.2 Hz frequency shift under exposure to 1 ppm formaldehyde vapor. The ΔF of the TiO_2 fibers coated QCM sensors exposed to

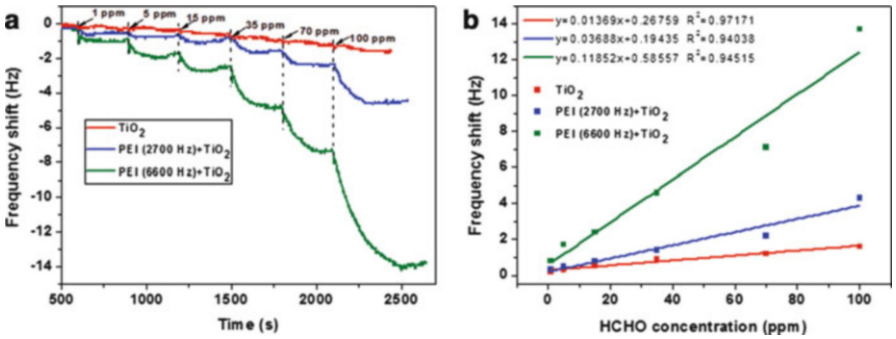

Fig. 1.9 Response of PEI@TiO_2 based QCM sensors with different PEI coating loads (i.e. 0, 2,700, 6,600 Hz) upon exposure to increasing formaldehyde concentrations (1–100 ppm) at ambient temperature of 25 °C (**a**). The frequency shift versus formaldehyde concentration. The coating load of TiO_2 was 1,300 Hz (**b**) (Reprinted with permission from [120]. © 2012 Elsevier Ltd)

5, 15, 35, 70 and 100 ppm of formaldehyde were 0.3, 0.5, 0.9, 1.2 and 1.6 Hz, respectively. It can be seen that the present PEI@TiO_2 based QCM sensor has not only the lowest detection limit (1 ppm) but also the fastest time response (<120 s). Figure 1.9b shows the ΔF values of sensors with different PEI coating loads (0, 2,700, and 6,600 Hz) in sensing formaldehyde with various concentrations of 1–100 ppm. The QCM isotherm to formaldehyde shows a Henry-type sorption at the concentration range [127]. This sorption behavior also proved the PEI@TiO_2 sensor possess a good linear relationship between frequency shift and concentration of formaldehyde which may give the sensors an extra advantage over their opponents.

1.3.1.3 PEI Functionalized PA-6 NFN Membranes Based Formaldehyde Sensors

Although the PEI@PS and PEI@TiO_2 membranes based QCM sensors have presented good performance to formaldehyde sensing, the detect limitation of above two sensors still cannot satisfy the WHO's standard. Facing with this obstacle, researchers turned their attention to explore new kind of substrates. Benefiting to several attractive features of NFN membranes such as extremely large specific surface area, high porosity, large stacking density and strongly tight adhesive force to the devices, it can lead to further enhancement in the facilitation of the analytes diffusion and oscillation transmission into the membranes, so as to detect formaldehyde at lower concentration level [83]. Recently, an effective formaldehyde detection system was developed by ESN depositing PA-6 NFN membranes on QCM and then modifying sensing PEI onto the NFN membranes (PEI@PA-6). As shown in Fig. 1.10d–f, the modification process did not disturb the NFN structure. When exposed to 100 ppm of formaldehyde, PEI@PA-6 NFN

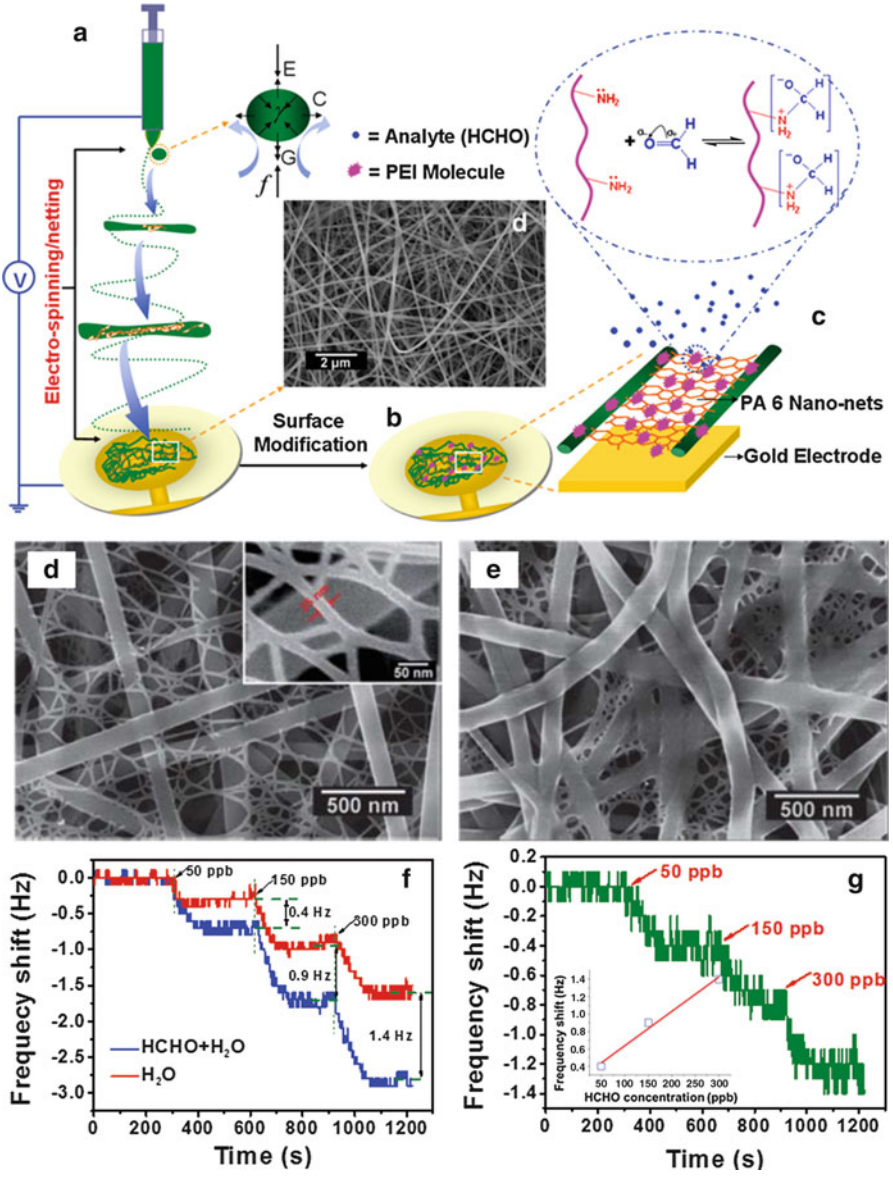

Fig. 1.10 Schematic diagram illustrating the fabrication of sensing layers on QCM. (**a**) ESN deposition of fibrous membranes onto the electrode of QCM. (**b**) Surface modification of NFN with diluted PEI solutions. (**c**) Illustration of PEI@PA-6 NFN on gold electrode and the reaction mechanism between formaldehyde and PEI. Typical FE-SEM image of PA-6 NFN membranes (**d**) and its corresponding samples modified with PEI (**e**). Responses of QCM-based PEI@PA-6 NFN (30 kV) sensors upon injection of water and the dilute formaldehyde solution, respectively (**f**). Response of the QCM sensor to formaldehyde (50, 150, and 300 ppb) (**g**), which derivate from (**f**) and removes effects of water. The inset in (**f**) shows the frequency shift versus the formaldehyde concentration (Reprinted with permission from [83]. © 2011 Royal Society of Chemistry)

(30 kV) based QCM sensor has achieved the largest response value, approximately three times as much as PEI flat film coated sensor. Subsequently, in order to detect formaldehyde with very low concentration, a moisture-compensating-based detecting method have been developed, i.e., firstly injected the dilute formaldehyde aqueous solution (1 wt%) into the chamber and then eliminated the influence of moisture. Figure 1.10f shows the responses of PEI@PA-6 NFN based QCM sensors upon injection of water and the dilute formaldehyde solution. The response of moisture-compensating QCM sensor exposing to formaldehyde was shown in Fig. 1.10g, indicating that the PEI@PA-6 NFN based QCM sensors exhibits a reduced detection limit for formaldehyde down to 50 ppb and a rapid response time (<100 s). In comparison with aforementioned works using QCM platform for formaldehyde sensing, the present PEI@PA-6 NFN based QCM sensors had not only the lowest detection limit but also the fastest time response, implying a high selectivity to formaldehyde and can be considered as an excellent candidate for gas sensing applications.

In addition to formaldehyde sensors, various kinds of QCM sensors based on electrospun nanofibers and NFN membranes have been developed such as sensors for humidity [99], trimethylamine [97], HCl [87] assaying and so on. There is no doubt that electrospun nanofibers have already become a desired substrate for QCM construction. Although the nanofibers based QCM sensors have gained an increased attention and achieved great progress. There is still a long distance from present condition to practical applications. Here are some possible reasons, first of all, the QCM system is still a little bit complex for people carrying around, so try to simplify the system and achieve the feature of direct reading are very important. Secondly, some performance of QCM system need further improve, including response time, stability, and reproducibility. Apart from QCM system, there are other structure features, such as viscoelastic, stiffness will influent the sensitivity waiting us to explore.

1.3.2 Colorimetric Sensors

Colorimetric sensors on patterned paper, fibrous material or plastic were developed as the least expensive, user-friendly alternative to conventional analytical instrumentations for 'point-of-care' medical diagnosis, environmental monitoring, and food quality control [128–131]. These low-cost platforms have been integrated with both colorimetric, and electrochemical detection systems. Such sensors are miniaturized and disposable and can be used for on-site analysis. In this section, we will focus on the application of electrospun nanofibers and NFN membranes on formaldehyde and heavy metal ions colorimetric sensing.

1.3.2.1 Colorimetric Strips for Formaldehyde Assaying

It goes without saying that the formaldehyde is one of most serious indoor air pollutant, can cause serious health damage. Wang et al. [132] demonstrated a label-free colorimetric sensor strip for real-time formaldehyde detection based on fluoral-p decorated PAN nanofibrous membranes. When the sensor strip was exposed to formaldehyde, the color of strips was dramatically changed from white to yellow attributed to the formation of symmetrically substituted 1, 4-dihydropyridines through the derived Hantzch reaction (Fig. 1.11a).

Because of selectivity is crucial for analytical chemistry grade, they systematically investigated the selectivity of the PAN/fuoral-p colorimetric strips by testing various VOCs (1 ppm) involving acetaldehyde, acetone, ethanol, dichloromethane, benzene, toluene, xylene, chloroform, ammonia, and DMF, which were possible interference vapors to assay. It is clearly observed from Fig. 1.11b that only formaldehyde induced a remarkable reflectance decrease at 417 nm and a distinct color change from white to yellow, implying that the interferential vapors have a negligible influence due to the specific reaction between formaldehyde and fuoral-p. It is worthwhile to note that acetaldehyde also cannot cause the color change, although acetaldehyde can also undergo the first stage with fuoral-p. This may be

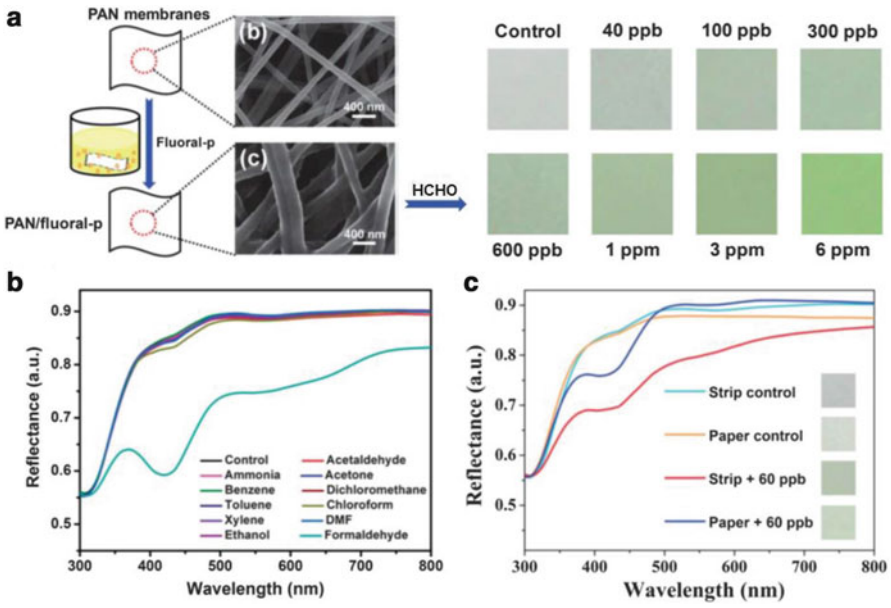

Fig. 1.11 The procedure for the fabrication of PAN/fluoral-p colorimetric sensor strips and the corresponding color changes after exposure to different concentration of HCHO (**a**). The UV-vis reflectance spectra of colorimetric strips after exposure to various VOCs (1 ppm) for 30 min (**b**). The UV-vis reflectance spectra and photographs of the PAN/fluoral-p nanofibrous strips and filter paper-based strips after exposure to 60 ppb formaldehyde (**c**) (Reprinted with permission from [132]. © 2013 Royal Society of Chemistry)

due to the fact that acetaldehyde molecules contain three active hydrogen atoms, the water molecule will be eliminated from methyl in the second stage which would lead to the formation of different end products (Mannich base), and so it would not induce the color change [133].

In corroboration of the superiority of electrospun nanofibers as the substrate, Wang et al. further compared their strips with the filter paper based strips. After espousing the PAN/fuoral-p nanofibrous strips and filter paper-based strips to 60 ppb formaldehyde under the optimized conditions. Figure 1.11c revealed that the reflectance intensity decrease at 417 nm of nanofibrous strips, substantially larger than filter paper strips which might be attributed to the large specific surface area and high porosity of fibrous membranes. Additionally, the corresponding color change of the nanofibrous membranes-based strips was much more obvious than the filter paper-based ones. Moving forward, this work also promotes a strategy for the design and development of versatile label-free colorimetric sensors toward various analytes in the future.

1.3.2.2 Colorimetric Strips for Mercury (II) Ions

Mercury, one of the most toxic metals, has drawn much attention due to its toxicity and impact on the public health. Mercury ions (Hg^{2+}) is released into the environment as a result of both natural processes and human activities, which can accumulate in the human body and readily penetrate through biological membranes, thus inactivating important cell functions and causing a wide variety of diseases such as brain damage, serious cognitive, motion disorders and Minamata disease [30, 134, 135]. Because of its high toxicity, Hg^{2+} ions has been included on the list of priority pollutants by U.S. EPA with a mandatory discharge limit of 50 nM for wastewater and a maximum concentration level of 10 nM for drinking water [136, 137]. Among the numerous analytical methods that are available for the detection of Hg^{2+} ions, colorimetric strategies offer distinct advantages in terms of sensitivity, selectivity, response time, and local observation.

Si et al. [109] report a novel, ultrasensitive, selective and flexible sensor strip based on PANI/PA-6/PVB NFN membranes for naked-eye colorimetric detection of Hg^{2+} ions in water. The sensing mechanism involves the transformations between different oxidation and doping forms of PANI. Figure 1.12a, b presents the changes of FE-SEM and optical images that accompany the treatment of PANI/PA-6/PVB NFN membranes with hydrazine aqueous solution. During the process, a series of redox and doping reactions took place. In the first stage, the benzenoid segments in leucoemeraldine base (fully reduced, PANI-LB) are oxidized by Hg^{2+} to form quinoid segment, yielding the emeraldine base (half oxidized, PANI-EB), thus inducing the first "turn-on" singles assigned to the charge transfer from the benzenoid to quinoid rings. Following, there are two competitive doping reaction of PANI-EB, protonation doping and Hg^{2+} complexation doping, and thus the color changed from green to blue vividly [138, 139]. Upon exposure to Hg^{2+} aqueous solution, the sensors exhibit two significant reflectance intensity decreasing bands

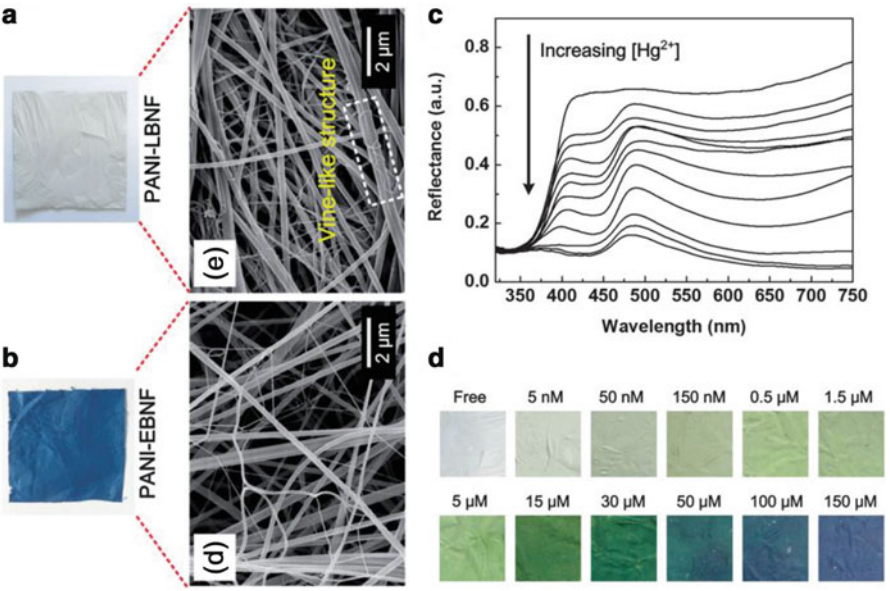

Fig. 1.12 FE-SEM and optical images of the PANI/PA-6/PVB NFN membranes (**a**) before (over) and (**b**) after (down) treated with hydrazine aqueous solution (40 wt%) for 2 h. (**c**) Reflectance spectra and (**d**) optical colorimetric response of the sensor strips after incubation for 20 min in Hg^{2+} aqueous solutions with concentrations of (0, 5 nM, 50 nM, 150 nM, 0.5 μM, 1.5 μM, 5 μM, 15 μM, 30 μM, 50 μM, 100 μM, and 150 μM) (Reprinted with permission from [109]. © 2014 Royal Society of Chemistry)

at 440 and 645 nm which induce the color changes from white to blue dramatically (Fig. 1.12c, d). This new sensor shows colorimetric response specifically to Hg^{2+} ions (white-to-blue color change) over other possible interfering metal cations and allows for detection of Hg^{2+} in aqueous solution with a low detection limit of 5 nM observing by naked eye.

The kinetic sensing response was also studied by continuously monitoring the reflectance spectra of sensor strips as a function of time after the addition of Hg^{2+}. It was found that the reflectance intensity of 440 nm decreased gradually over the entire time range, meanwhile the intensity of 645 nm showed a relatively stable region (>7 min) after the first slight decrease (Fig. 1.13a), thus leading to a continuous enhancement of the yellow/green color (Fig. 1.14c). This result suggests that the oxidation of benzenoid segments would be slowly saturated due to the weak oxidizability of the solution with low Hg^{2+} concentration (e.g., 5 μM), while the doping of quinoid rings (either protonation or Hg^{2+} complexation) was a constant, ongoing process. More interestingly, the dynamic responses upon exposure to high Hg^{2+} concentration (e.g., 150 μM) exhibited a dramatic difference from that of 5 μM. As shown in Fig. 1.13b, the reflectance intensity of 440 nm further decreased owing to the strong complexation doping with a large amount of Hg^{2+}. A rapid decrease of the intensity at 645 nm was also observed and it reached almost 0 after

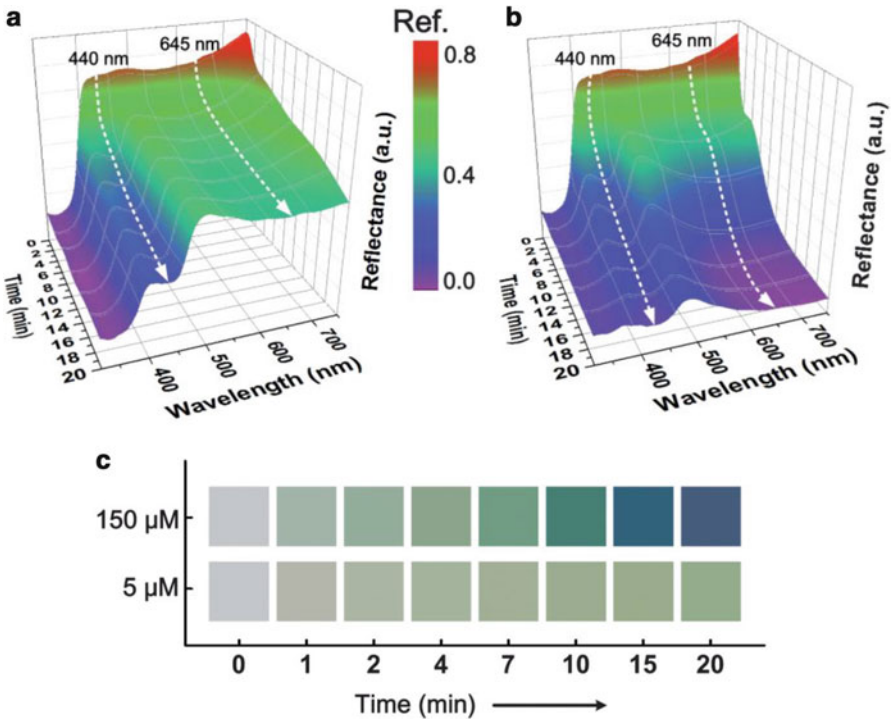

Fig. 1.13 The kinetic reflectance response of the PANI-LBNF sensor strips as a function of time for different Hg^{2+} concentrations: (**a**) 5 μM and (**b**) 150 μM. (**c**) The corresponding time dependent visualization of CIELAB color changes *versus* Hg^{2+} concentration (Reprinted with permission from [109]. © 2014 Royal Society of Chemistry)

15 min, indicating a complete oxidation of benzenoid segments into fully oxidized PANI-PB, and finally resulted in the vivid blue color [140].

1.3.2.3 Colorimetric Strips for Lead (II) Ions

Lead ion (Pb^{2+}) is another ubiquitous metallic pollutant in the environment and had been used recklessly until very recently. Nowadays, lead pollution has become a persisting problem and caused a long-lasting danger to human health. Even very low level of lead exposure can correspondingly result in high blood pressure, neurological, cardiovascular and hypertension developmental disorders, which lead to particularly serious problems in children including slowed motor responses, IQ decreasing and developmental disorders hypertension [141–143]. The Centers for Disease Control and Prevention has defined that the whole blood lead concentration >0.48 μM (100 μg/L) in children as indicative of significant exposure and recommends chelation therapy [144]. Due to the toxicity of Pb^{2+}, it is highly

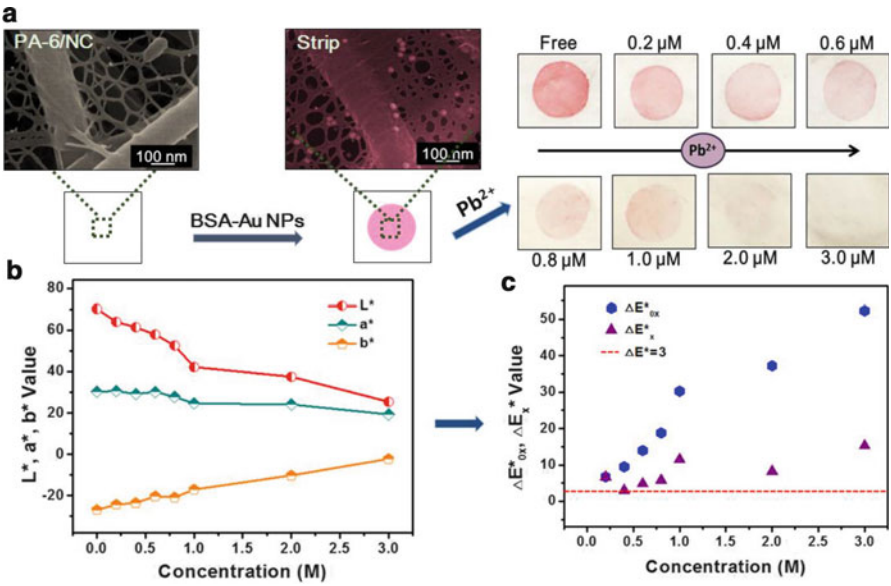

Fig. 1.14 (**a**) Schematic illustration of the colorimetric detection of Pb^{2+} based on the PA-6/NC NFN membranes and corresponding optical images of strips after incubated with different concentration of Pb^{2+} solution for 30 min at 60 °C. (**b**) The $L^*a^*b^*$ values converted from the UV-vis absorbance spectra of colorimetric strips variation *versus* the concentration of Pb^{2+}. (**c**) ΔE_x^* (color-difference of adjacent detecting samples) and ΔE_{0x}^* (the color-difference between detecting samples and free sample) calculated from $L^*a^*b^*$ values *versus* a series of Pb^{2+} concentrations (Reprinted with permission from [110]. © 2013 Elsevier Ltd)

desirable to develop a portable, easy use, house-hold use on-site, selective and sensitive method for Pb^{2+} assaying.

Li et al. [110] developed a simple colorimetric strip for assaying Pb^{2+}, constructed by immobilizing bovine serum albumin (BSA) decorated Au NPs (BAu probe) on PA-6/NC NFN membrane, which fabricated *via* multi-jet electrospinning. As shown in Fig. 1.14a, the successfully spotting BAu probe on PA-6/NC NFN membranes was confirmed by FE-SEM image. After the leaching liquor (pH = 10, 0.27 M $Na_2S_2O_3$ and 0.25 M 2-mercaptoethanol) was spiked with various concentrations of Pb^{2+} and incubated for 30 min, the color of strips gradually fade away from deep pink to white which is attribute to the fact that Pb^{2+} ions accelerate the leaching rate of Au NPs induced by $S_2O_3^{2-}$ and 2-mercaptoethanol [145].

In order to further quantitatively investigate the color-difference between two detecting samples as displayed in Fig. 1.14a, a converting method was used to convert a UV-vis absorbance spectrum into $L^*a^*b^*$ values for given illuminant. In this work, the CIE normalized D65 is used, which closely matches that of the sky daylight. ΔE_x^* (the color-difference of two adjacent detecting samples) and ΔE_0x^* (the color-difference between detecting samples to free sample), is calculated in L^*,

a^* and b^*. ΔE is defined as the Euclidean distance between these two sets of color coordinates, were evaluated as [146, 147],

$$\Delta E*_x = \sqrt{(L*_x - L*_{x-1})^2 + (a*_x - a*_{x-1})^2 + (b*_x - b*_{x-1})^2} \tag{1.2}$$

$$\Delta E_0*_x = \sqrt{(L*_x - L*_0)^2 + (a*_x - a*_0)^2 + (b*_x - b*_0)^2} \tag{1.3}$$

As shown in Fig. 1.14c, the values of ΔE_{0x}* and ΔE_x* *versus* Pb^{2+} concentration revealed in Fig. 1.14a, all the results obtained were higher than 3 CIE LAB units, which could readily be identified by naked eyes.

The further, In addition, they compared two kinds of substrates here to evaluate the performance of the NFN membranes. As shown in Fig. 1.15c, the UV-vis absorbance spectra and photographs of NC based colorimetric film after incubated in optimized leaching liquor (0.27 M $Na_2S_2O_3$, 0.25 M 2-ME) spiked with 1 μM Pb^{2+}. The colorimetric responses of film obtained were substantially lower than strip and it was conspicuous that the ΔE_{0film}* could hardly be appreciated by human eyes. Because the strips have approximately one to two orders of magnitude larger surface area than that of films, which supplied more active sites. Apart from that, the morphology of film showed in Fig. 1.15a, b also gave a reasonably good explanation of less BAu probes binding amount. After analyzing the FE-SEM image, it was shown that the through-hole width distribute in range of 0.25–3 μm (major in micropore range) within the film. Unlike NFN membranes, the nanofibers overlap each other in a completely random manner during electrospinning procedure, giving a rise to the silt-shape pore structure which is ideal for membranes binding BAu probe.

1.4 Summary and Perspectives

In summary, this chapter presents a comprehensive review of the progress in QCM and colorimetric sensors based on electrospinning-netting nanofibers/nets. In virtue of the large surface-area-to-volume ratio, high length-to-diameter ratio, tailored pore structure, large stacking density, nanofiber-based sensors achieved high sensitivity, fast response and recovery, excellent stability. In further study, the following aspects should be taken into consideration: for QCM sensors, the sensing materials need further explore. Since the interfacial parameters, like roughness, surface free energy and surface charge will confound the responses of sensors, further regulate is also very important. In addition, there are other structure features, such as viscoelastic, stiffness will influent the sensitivity waiting us to explore. For colorimetric sensors, it still have a lot of problems need we to explore. How to decrease the response time? How to achieve the long-term storage, and how to improve the loading uniformity and fastness are still waiting for us to figure out. Furthermore, the structure of nanofibers also need further regulate. For instance,

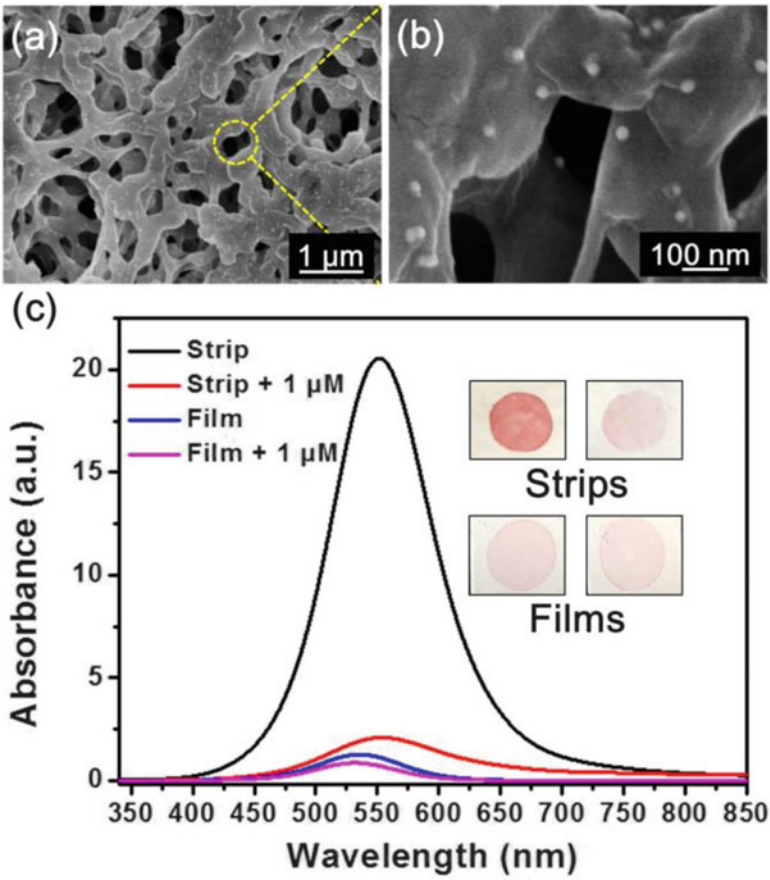

Fig. 1.15 UV-vis spectra and colorimetric responses of the colorimetric strips and commercial NC films having been incubated in two leaching liquors added with 0 and 1 μM Pb^{2+}, respectively (Reprinted with permission from [110]. © 2013 Elsevier Ltd)

high porosity and large SSA. Moving forward, it is reasonable to believe the electrospun nanofiber-based sensors may throw a light on the development of sensors in future.

Acknowledgement This work is supported by the National Basic Research Program of China (973 Program, 2012CB525005), the National Natural Science Foundation of China (No. 51173022, 51273038 and 51322304), the Huo Yingdong Foundation (131070), the Program for New Century Talents of the University in China, the Fundamental Research Funds for the Central Universities, and the "DHU Distinguished Young Professor Program".

References

1. C.D. Holmes, Air pollution and forest water use. Nature **507**(7491), E1–E2 (2014). doi:10.1038/nature13113
2. C.C. Macpherson, Climate change matters. J. Med. Ethics **40**(4), 288–290 (2014). doi:10.1136/medethics-2012-101084
3. S. Rodrıguez, X. Querol, A. Alastuey, M.-M. Viana, M. Alarcón, E. Mantilla, C.R. Ruiz, Comparative PM10–PM2.5 source contribution study at rural, urban and industrial sites during PM episodes in Eastern Spain. Sci. Total Environ. **328**(1–3), 95–113 (2004). doi:http://dx.doi.org/10.1016/S0048-9697(03)00411-X
4. M. Kampa, E. Castanas, Human health effects of air pollution. Environ. Pollut. **151**(2), 362–367 (2008). doi:http://dx.doi.org/10.1016/j.envpol.2007.06.012
5. P.D. Noyes, M.K. McElwee, H.D. Miller, B.W. Clark, L.A. Van Tiem, K.C. Walcott, K.N. Erwin, E.D. Levin, The toxicology of climate change: environmental contaminants in a warming world. Environ. Int. **35**(6), 971–986 (2009). doi:http://dx.doi.org/10.1016/j.envint.2009.02.006
6. W. Gan, M. Koehoorn, H. Davies, P. Demers, L. Tamburic, M. Brauer, Long-term exposure to traffic-related air pollution and the risk of coronary heart disease hospitalization and mortality. Epidemiology **22**(1), S30 (2011). doi:10.1097/1001.ede.0000391750.0000338925.0000391750f
7. P. Brown, *Toxic Exposures: Contested Illnesses and the Environmental Health Movement* (Columbia University Press, New York, 2013)
8. F. Fu, Q. Wang, Removal of heavy metal ions from wastewaters: a review. J. Environ. Manage. **92**(3), 407–418 (2011). doi:http://dx.doi.org/10.1016/j.jenvman.2010.11.011
9. B. Wei, L. Yang, A review of heavy metal contaminations in urban soils, urban road dusts and agricultural soils from China. Microchem. J. **94**(2), 99–107 (2010). doi:http://dx.doi.org/10.1016/j.microc.2009.09.014
10. C. Luo, C. Liu, Y. Wang, X. Liu, F. Li, G. Zhang, X. Li, Heavy metal contamination in soils and vegetables near an e-waste processing site, south China. J. Hazard. Mater. **186**(1), 481–490 (2011). doi:http://dx.doi.org/10.1016/j.jhazmat.2010.11.024
11. B.R. Gurjar, A. Jain, A. Sharma, A. Agarwal, P. Gupta, A.S. Nagpure, J. Lelieveld, Human health risks in megacities due to air pollution. Atmos. Environ. **44**(36), 4606–4613 (2010). doi:http://dx.doi.org/10.1016/j.atmosenv.2010.08.011
12. H. Kan, R. Chen, S. Tong, Ambient air pollution, climate change, and population health in China. Environ. Int. **42**(0), 10–19 (2012). doi:http://dx.doi.org/10.1016/j.envint.2011.03.003
13. M.H. Yu, H. Tsunoda, M. Tsunoda, *Environmental Toxicology: Biological and Health Effects of Pollutants*, 3rd edn. (Taylor & Francis, Boca Raton, 2011)
14. L.B. Lave, E.P. Seskin, *Air Pollution and Human Health* (Taylor & Francis, Boca Raton, 2013)
15. N.Z. Muller, R. Mendelsohn, W. Nordhaus, Environmental accounting for pollution in the United States economy. Am. Econ. Rev. **101**(5), 1649–1675 (2011). doi:10.1257/aer.101.5.1649
16. T. Kjellstrom, A. Butler, R. Lucas, R. Bonita, Public health impact of global heating due to climate change: potential effects on chronic non-communicable diseases. Int. J. Public Health **55**(2), 97–103 (2010). doi:10.1007/s00038-009-0090-2
17. World Health Organization, UNICEF, Water Supply and Sanitation Collaborative Council, WHO/UNICEF Joint Water Supply and Sanitation Monitoring Programme, *Global Water Supply and Sanitation Assessment 2000 Report* (World Health Organization, Geneva, 2000)
18. Y.F. Lee, C.C. Huang, Colorimetric assay of lead ions in biological samples using a nanogold-based membrane. ACS Appl. Mater. Interfaces **3**(7), 2747–2754 (2011). doi:10.1021/am200535s
19. T. Jasarevic, G. Thomas, N. Osseiran, 7 million premature deaths annually linked to air pollution (2014), http://www.who.int/mediacentre/news/releases/2014/air-pollution/en/

20. L.D. Zhang, X.S. Fang, Controlled growth and characterization methods of semiconductor nanomaterials. J. Nanosci. Nanotechnol. **8**(1), 149–201 (2008). doi:10.1166/jnn.2008.N02
21. R. Purkhart, A. Hillmann, R. Graupner, G. Becher, Detection of characteristic clusters in IMS-Spectrograms of exhaled air polluted with environmental contaminants. Int. J. Ion Mobil. Spectrom. **15**(2), 63–68 (2012). doi:10.1007/s12127-012-0090-4
22. A. Masiá, J. Campo, C. Blasco, Y. Picó, Ultra-high performance liquid chromatography–quadrupole time-of-flight mass spectrometry to identify contaminants in water: an insight on environmental forensics. J. Chromatogr. A **1345**(0), 86–97 (2014). doi:http://dx.doi.org/10.1016/j.chroma.2014.04.017
23. C. Arpa Şahin, M. Efeçınar, N. Şatıroğlu, Combination of cloud point extraction and flame atomic absorption spectrometry for preconcentration and determination of nickel and manganese ions in water and food samples. J. Hazard. Mater. **176**(1–3), 672–677 (2010). doi:http://dx.doi.org/10.1016/j.jhazmat.2009.11.084
24. J.C. Van Loon, *Analytical Atomic Absorption Spectroscopy: Selected Methods* (Academic, New York, 1980)
25. K.C. Armstrong, C.E. Tatum, R.N. Dansby-Sparks, J.Q. Chambers, Z.-L. Xue, Individual and simultaneous determination of lead, cadmium, and zinc by anodic stripping voltammetry at a bismuth bulk electrode. Talanta **82**(2), 675–680 (2010). doi:http://dx.doi.org/10.1016/j.talanta.2010.05.031
26. Z. Bi, P. Salaün, C.M.G. van den Berg, Study of bare and mercury-coated vibrated carbon, gold and silver microwire electrodes for the determination of lead and cadmium in seawater by anodic stripping voltammetry. Electroanalysis **25**(2), 357–366 (2013). doi:10.1002/elan.201200446
27. A. Cavazzini, L. Pasti, A. Massi, N. Marchetti, F. Dondi, Recent applications in chiral high performance liquid chromatography: a review. Anal. Chim. Acta **706**(2), 205–222 (2011). doi:http://dx.doi.org/10.1016/j.aca.2011.08.038
28. T. Wagner, S. Haffer, C. Weinberger, D. Klaus, M. Tiemann, Mesoporous materials as gas sensors. Chem. Soc. Rev. **42**(9), 4036–4053 (2013). doi:10.1039/C2CS35379B
29. A. Afzal, N. Iqbal, A. Mujahid, R. Schirhagl, Advanced vapor recognition materials for selective and fast responsive surface acoustic wave sensors: a review. Anal. Chim. Acta **787**(0), 36–49 (2013). doi:http://dx.doi.org/10.1016/j.aca.2013.05.005
30. A.N. Uglov, A. Bessmertnykh-Lemeune, R. Guilard, A.D. Averin, I.P. Beletskaya, Optical methods for the detection of heavy metal ions. Russ. Chem. Rev. **83**(3), 196 (2014)
31. A. Allouch, S. Le Calvé, C.A. Serra, Portable, miniature, fast and high sensitive real-time analyzers: BTEX detection. Sens. Actuators B **182**(0), 446–452 (2013). doi:http://dx.doi.org/10.1016/j.snb.2013.03.010
32. A. Wilson, Diverse applications of electronic-nose technologies in agriculture and forestry. Sensors **13**(2), 2295–2348 (2013)
33. F. Long, A. Zhu, H. Shi, Recent advances in optical biosensors for environmental monitoring and early warning. Sensors **13**(10), 13928–13948 (2013)
34. S. Su, W. Wu, J. Gao, J. Lu, C. Fan, Nanomaterials-based sensors for applications in environmental monitoring. J. Mater. Chem. **22**(35), 18101–18110 (2012). doi:10.1039/C2JM33284A
35. L. Zhang, M. Fang, Nanomaterials in pollution trace detection and environmental improvement. Nano Today **5**(2), 128–142 (2010). doi:http://dx.doi.org/10.1016/j.nantod.2010.03.002
36. A. Vaseashta, M. Vaclavikova, S. Vaseashta, G. Gallios, P. Roy, O. Pummakarnchana, Nanostructures in environmental pollution detection, monitoring, and remediation. Sci. Technol. Adv. Mater. **8**(1–2), 47 (2007)
37. B.S. Kim, I.S. Kim, Recent nanofiber technologies. Polym. Rev. **51**(3), 235–238 (2011). doi:10.1080/15583724.2011.599507
38. J. Miao, M. Miyauchi, T.J. Simmons, J.S. Dordick, R.J. Linhardt, Electrospinning of nanomaterials and applications in electronic components and devices. J. Nanosci. Nanotechnol. **10**(9), 5507–5519 (2010). doi:10.1166/jnn.2010.3073

39. B. Ding, M. Wang, J. Yu, G. Sun, Gas sensors based on electrospun nanofibers. Sensors **9**(3), 1609–1624 (2009). doi:10.3390/s90301609
40. D. Li, Y. Xia, Electrospinning of nanofibers: reinventing the wheel? Adv. Mater. **16**(14), 1151–1170 (2004). doi:10.1002/adma.200400719
41. H.R. Darrell, C. Iksoo, Nanometre diameter fibres of polymer, produced by electrospinning. Nanotechnology **7**(3), 216 (1996)
42. P. Zahedi, I. Rezaeian, S.-O. Ranaei-Siadat, S.-H. Jafari, P. Supaphol, A review on wound dressings with an emphasis on electrospun nanofibrous polymeric bandages. Polym. Adv. Technol. **21**(2), 77–95 (2010). doi:10.1002/pat.1625
43. M. Inagaki, Y. Yang, F. Kang, Carbon nanofibers prepared via electrospinning. Adv. Mater. **24**(19), 2547–2566 (2012). doi:10.1002/adma.201104940
44. P. Ramesh Kumar, N. Khan, S. Vivekanandhan, N. Satyanarayana, A.K. Mohanty, M. Misra, Nanofibers: effective generation by electrospinning and their applications. J. Nanosci. Nanotechnol. **12**(1), 1–25 (2012). doi:10.1166/jnn.2012.5111
45. W.D. Luedtke, U. Landman, Y.H. Chiu, D.J. Levandier, R.A. Dressler, S. Sok, M.S. Gordon, Nanojets, electrospray, and ion field evaporation: molecular dynamics simulations and laboratory experiments. J. Phys. Chem. A **112**(40), 9628–9649 (2008). doi:10.1021/jp804585y
46. N. Bhardwaj, S.C. Kundu, Electrospinning: a fascinating fiber fabrication technique. Biotechnol. Adv. **28**(3), 325–347 (2010). doi:http://dx.doi.org/10.1016/j.biotechadv.2010.01.004
47. B. Ding, H.Y. Kim, S.C. Lee, D.R. Lee, K.J. Choi, Preparation and characterization of nanoscaled poly(vinyl alcohol) fibers via electrospinning. Fibers and Polymers **3**(2), 73–79 (2002). doi:10.1007/BF02875403
48. B. Kim, H. Park, S.H. Lee, W.M. Sigmund, Poly(acrylic acid) nanofibers by electrospinning. Mater. Lett. **59**(7), 829–832 (2005). doi:http://dx.doi.org/10.1016/j.matlet.2004.11.032
49. X. Li, L. Lin, Y. Zhu, W. Liu, T. Yu, M. Ge, Preparation of ultrafine fast-dissolving cholecalciferol-loaded poly(vinyl pyrrolidone) fiber mats via electrospinning. Polym. Compos. **34**(2), 282–287 (2013). doi:10.1002/pc.22402
50. C. Chen, L. Wang, Y. Huang, Electrospinning of thermo-regulating ultrafine fibers based on polyethylene glycol/cellulose acetate composite. Polymer **48**(18), 5202–5207 (2007). doi:http://dx.doi.org/10.1016/j.polymer.2007.06.069
51. D. Li, Y. Xia, Fabrication of titania nanofibers by electrospinning. Nano Lett. **3**(4), 555–560 (2003). doi:10.1021/nl034039o
52. A. Nikfarjam, S. Fardindoost, A. Iraji zad, Fabrication of Pd Doped WO3 nanofiber as hydrogen sensor. Polymers **5**(1), 45–55 (2013)
53. M. Fan, W. Hui, Z. Li, Z. Shen, H. Li, A. Jiang, Y. Chen, R. Liu, Fabrication and piezoresponse of electrospun ultra-fine $Pb(Zr_{0.3}, Ti_{0.7})O_3$ nanofibers. Microelectron. Eng. **98**(0), 371–373 (2012). doi:http://dx.doi.org/10.1016/j.mee.2012.07.026
54. L. Deng, R.J. Young, I.A. Kinloch, Y. Zhu, S.J. Eichhorn, Carbon nanofibres produced from electrospun cellulose nanofibres. Carbon **58**(0), 66–75 (2013). doi:http://dx.doi.org/10.1016/j.carbon.2013.02.032
55. H. Yan, N.K. Mahanta, B. Wang, S. Wang, A.R. Abramson, M. Cakmak, Structural evolution in graphitization of nanofibers and mats from electrospun polyimide–mesophase pitch blends. Carbon **71**(0), 303–318 (2014). doi:http://dx.doi.org/10.1016/j.carbon.2014.01.057
56. Y. Si, T. Ren, Y. Li, B. Ding, J. Yu, Fabrication of magnetic polybenzoxazine-based carbon nanofibers with Fe3O4 inclusions with a hierarchical porous structure for water treatment. Carbon **50**(14), 5176–5185 (2012). doi:http://dx.doi.org/10.1016/j.carbon.2012.06.059
57. A. Khalil, R. Hashaikeh, M. Jouiad, Synthesis and morphology analysis of electrospun copper nanowires. J. Mater. Sci. **49**(8), 3052–3065 (2014). doi:10.1007/s10853-013-8005-2
58. V. Thavasi, G. Singh, S. Ramakrishna, Electrospun nanofibers in energy and environmental applications. Energy Environ. Sci. **1**(2), 205–221 (2008). doi:10.1039/B809074M

59. D. Bin, Y. Jianyong, *Electrospinning and Nanofibers* (China Textile & Apparel Press, Beijing, 2011)
60. C. Tran, V. Kalra, Co-continuous nanoscale assembly of Nafion-polyacrylonitrile blends within nanofibers: a facile route to fabrication of porous nanofibers. Soft Matter **9**(3), 846–852 (2013). doi:10.1039/C2SM25976A
61. Y. Yao, W. Yin, J. Cao, M. Yang, J. Li, S. Zhao, Y. Li, X. He, J. Leng, Manipulation and formation mechanism of silica one-dimensional periodic structures by roller electrospinning. Langmuir **30**(9), 2335–2345 (2014). doi:10.1021/la4037277
62. Q. Du, D.R. Harding, H. Yang, Helical peanut-shaped poly(vinyl pyrrolidone) ribbons generated by electrospinning. Polymer **54**(25), 6752–6759 (2013). doi:http://dx.doi.org/10.1016/j.polymer.2013.10.029
63. S. Li, J. Leng, Y. Fan, C. Fu, H. Shen, Y. Xue, D. Xu, Electrospinning synthesis and structural characterization of manganese oxyborate (Mn2OBO3) necklace-like nanofibers. Phys. Status Solidi A **208**(1), 114–117 (2011). doi:10.1002/pssa.201026499
64. J. Li, K.I. Lee, X. Lu, S. Bao, T. Hua, J.H. Xin, B. Fei, In-situ growth of pine-needle-like tungsten oxide nanowire arrays on carbon nanofibers. Mater. Lett. **99**(0), 131–133 (2013). doi:http://dx.doi.org/10.1016/j.matlet.2013.02.077
65. Z. Chang, "Firecracker-shaped" ZnO/polyimide hybrid nanofibers viaelectrospinning and hydrothermal process. Chem. Commun. **47**(15), 4427–4429 (2011). doi:10.1039/C0CC05634K
66. H.-Y. Chen, T.-L. Zhang, J. Fan, D.-B. Kuang, C.-Y. Su, Electrospun hierarchical TiO2 nanorods with high porosity for efficient dye-sensitized solar cells. ACS Appl. Mater. Interfaces **5**(18), 9205–9211 (2013). doi:10.1021/am402853q
67. H. Chen, N. Wang, J. Di, Y. Zhao, Y. Song, L. Jiang, Nanowire-in-microtube structured core/shell fibers via multifluidic coaxial electrospinning. Langmuir **26**(13), 11291–11296 (2010). doi:10.1021/la100611f
68. F. Mou, J.-G. Guan, W. Shi, Z. Sun, S. Wang, Oriented contraction: a facile nonequilibrium heat-treatment approach for fabrication of maghemite fiber-in-tube and tube-in-tube nanostructures. Langmuir **26**(19), 15580–15585 (2010). doi:10.1021/la102830p
69. J. Lin, B. Ding, J. Yang, J. Yu, G. Sun, Subtle regulation of the micro- and nanostructures of electrospun polystyrene fibers and their application in oil absorption. Nanoscale **4**(1), 176–182 (2012). doi:10.1039/c1nr10895f
70. D. Li, Y. Xia, Direct fabrication of composite and ceramic hollow nanofibers by electrospinning. Nano Lett. **4**(5), 933–938 (2004). doi:10.1021/nl049590f
71. J. Lin, B. Ding, J. Yu, Y. Hsieh, Direct fabrication of highly nanoporous polystyrene fibers via electrospinning. ACS Appl. Mater. Interfaces **2**(2), 521–528 (2010). doi:10.1021/am900736h
72. B. Ding, M. Wang, X. Wang, J. Yu, G. Sun, Electrospun nanomaterials for ultrasensitive sensors. Mater. Today **13**(11), 16–27 (2010). doi:http://dx.doi.org/10.1016/S1369-7021(10)70200-5
73. J. Wu, N. Wang, Y. Zhao, L. Jiang, Electrospinning of multilevel structured functional micro-/nanofibers and their applications. J. Mater. Chem. A **1**(25), 7290–7305 (2013). doi:10.1039/C3TA10451F
74. D. Li, Y. Wang, Y. Xia, Electrospinning of polymeric and ceramic nanofibers as uniaxially aligned arrays. Nano Lett. **3**(8), 1167–1171 (2003). doi:10.1021/nl0344256
75. S.J. Cho, B. Kim, T. An, G. Lim, Replicable multilayered nanofibrous patterns on a flexible film. Langmuir **26**(18), 14395–14399 (2010). doi:10.1021/la102467u
76. D. Zhang, J. Chang, Patterning of electrospun fibers using electroconductive templates. Adv. Mater. **19**(21), 3664–3667 (2007). doi:10.1002/adma.200700896
77. M. Abbasipour, R. Khajavi, Nanofiber bundles and yarns production by electrospinning: a review. Adv. Polym. Technol. **32**(3), n/a–n/a (2013). doi:10.1002/adv.21363
78. G. Sun, D. Wei, X. Liu, Y. Chen, M. Li, D. He, J. Zhong, Novel biodegradable electrospun nanofibrous P(DLLA-CL) balloons for the treatment of vertebral compression fractures.

Nanomed. Nanotechnol. Biol. Med.. **9**(6), 829–838 (2013). doi:http://dx.doi.org/10.1016/j.nano.2012.12.003
79. A.M. Behrens, B.J. Casey, M.J. Sikorski, K.L. Wu, W. Tutak, A.D. Sandler, P. Kofinas, In situ deposition of PLGA nanofibers via solution blow spinning. ACS Macro Lett. **3**(3), 249–254 (2014). doi:10.1021/mz500049x
80. D. Ahirwal, A. Hebraud, R. Kadar, M. Wilhelm, G. Schlatter, From self-assembly of electrospun nanofibers to 3D cm thick hierarchical foams. Soft Matter **9**(11), 3164–3172 (2013). doi:10.1039/C2SM27543K
81. J. He, Y. Zhou, K. Qi, L. Wang, P. Li, S. Cui, Continuous twisted nanofiber yarns fabricated by double conjugate electrospinning. Fibers Polym. **14**(11), 1857–1863 (2013). doi:10.1007/s12221-013-1857-x
82. T. Wee-Eong, I. Ryuji, R. Seeram, Technological advances in electrospinning of nanofibers. Sci. Technol. Adv. Mater. **12**(1), 013002 (2011)
83. B. Ding, X. Wang, J. Yu, M. Wang, Polyamide 6 composite nano-fiber/net functionalized by polyethyleneimine on quartz crystal microbalance for highly sensitive formaldehyde sensors. J. Mater. Chem. **21**(34), 12784–12792 (2011). doi:10.1039/c1jm11847a
84. K. Lin, K.-N. Chua, G.T. Christopherson, S. Lim, H.-Q. Mao, Reducing electrospun nanofiber diameter and variability using cationic amphiphiles. Polymer **48**(21), 6384–6394 (2007). doi:http://dx.doi.org/10.1016/j.polymer.2007.08.056
85. H. Chaobo, C. Shuiliang, L. Chuilin, H.R. Darrell, Q. Haiyan, Y. Ying, H. Haoqing, Electrospun polymer nanofibres with small diameters. Nanotechnology **17**(6), 1558 (2006). doi:10.1088/0957-4484/17/6/004
86. X. Wang, B. Ding, G. Sun, M. Wang, J. Yu, Electro-spinning/netting: a strategy for the fabrication of three-dimensional polymer nano-fiber/nets. Prog. Mater. Sci. **58**(8), 1173–1243 (2013). doi:http://dx.doi.org/10.1016/j.pmatsci.2013.05.001
87. X. Wang, J. Wang, Y. Si, B. Ding, J. Yu, G. Sun, W. Luo, G. Zheng, Nanofiber-net-binary structured membranes for highly sensitive detection of trace HCl gas. Nanoscale **4**(23), 7585–7592 (2012). doi:10.1039/c2nr32730a
88. N.A.M. Barakat, M.A. Kanjwal, F.A. Sheikh, H.Y. Kim, Spider-net within the N6, PVA and PU electrospun nanofiber mats using salt addition: novel strategy in the electrospinning process. Polymer **50**(18), 4389–4396 (2009). doi:http://dx.doi.org/10.1016/j.polymer.2009.07.005
89. H.R. Pant, M.P. Bajgai, K.T. Nam, K.H. Chu, S.-J. Park, H.Y. Kim, Formation of electrospun nylon-6/methoxy poly(ethylene glycol) oligomer spider-wave nanofibers. Mater. Lett. **64**(19), 2087–2090 (2010). doi:http://dx.doi.org/10.1016/j.matlet.2010.06.047
90. H.R. Pant, M.P. Bajgai, C. Yi, R. Nirmala, K.T. Nam, W.-i. Baek, H.Y. Kim, Effect of successive electrospinning and the strength of hydrogen bond on the morphology of electrospun nylon-6 nanofibers. Colloids Surf. A Physicochem. Eng. Asp. **370**(1–3), 87–94 (2010). doi:http://dx.doi.org/10.1016/j.colsurfa.2010.08.051
91. S.Y. Tsou, H.S. Lin, C. Wang, Studies on the electrospun Nylon 6 nanofibers from polyelectrolyte solutions: 1. Effects of solution concentration and temperature. Polymer **52**(14), 3127–3136 (2011). doi:http://dx.doi.org/10.1016/j.polymer.2011.05.010
92. B. Ding, C. Li, Y. Miyauchi, O. Kuwaki, S. Shiratori, Formation of novel 2D polymer nanowebs via electrospinning. Nanotechnology **17**(15), 3685–3691 (2006). doi:10.1088/0957-4484/17/15/011
93. C. Mit-uppatham, M. Nithitanakul, P. Supaphol, Ultrafine electrospun polyamide-6 fibers: effect of solution conditions on morphology and average fiber diameter. Macromol. Chem. Phys. **205**(17), 2327–2338 (2004). doi:10.1002/macp.200400225
94. R.P.A. Hartman, D.J. Brunner, D.M.A. Camelot, J.C.M. Marijnissen, B. Scarlett, Jet break-up in electrohydrodynamic atomization in the cone-jet mode. J. Aerosol Sci. **31**(1), 65–95 (2000). doi:http://dx.doi.org/10.1016/S0021-8502(99)00034-8
95. R.L. Grimm, J.L. Beauchamp, Dynamics of field-induced droplet ionization: time-resolved studies of distortion, jetting, and progeny formation from charged and neutral methanol

droplets exposed to strong electric fields. J. Phys. Chem. B **109**(16), 8244–8250 (2005). doi:10.1021/jp0450540
96. J. Hu, X. Wang, B. Ding, J. Lin, J. Yu, G. Sun, One-step electro-spinning/netting technique for controllably preparing polyurethane nano-fiber/net. Macromol. Rapid Commun. **32**(21), 1729–1734 (2011). doi:10.1002/marc.201100343
97. X. Wang, B. Ding, J. Yu, Y. Si, S. Yang, G. Sun, Electro-netting: fabrication of two-dimensional nano-nets for highly sensitive trimethylamine sensing. Nanoscale **3**(3), 911–915 (2011). doi:10.1039/c0nr00783h
98. S. Yang, X. Wang, B. Ding, J. Yu, J. Qian, G. Sun, Controllable fabrication of soap-bubble-like structured polyacrylic acid nano-nets via electro-netting. Nanoscale **3**(2), 564–568 (2011). doi:10.1039/c0nr00730g
99. X. Wang, B. Ding, J. Yu, M. Wang, Highly sensitive humidity sensors based on electro-spinning/netting a polyamide 6 nano-fiber/net modified by polyethyleneimine. J. Mater. Chem. **21**(40), 16231–16238 (2011). doi:10.1039/c1jm13037d
100. X. Wang, Y. Si, J. Wang, B. Ding, J. Yu, S.S. Al-Deyab, A facile and highly sensitive colorimetric sensor for the detection of formaldehyde based on electro-spinning/netting nano-fiber/nets. Sens Actuators B Chem. **163**(1), 186–193 (2012). doi:10.1016/j.snb.2012.01.033
101. N. Wang, X. Wang, B. Ding, J. Yu, G. Sun, Tunable fabrication of three-dimensional polyamide-66 nano-fiber/nets for high efficiency fine particulate filtration. J. Mater. Chem. **22**(4), 1445–1452 (2012). doi:10.1039/c1jm14299b
102. X. Wang, B. Ding, J. Yu, M. Wang, F. Pan, A highly sensitive humidity sensor based on a nanofibrous membrane coated quartz crystal microbalance. Nanotechnology **21**(5), 055502 (2010). doi:10.1088/0957-4484/21/5/055502
103. N. Wang, X. Wang, Y. Jia, X. Li, J. Yu, B. Ding, Electrospun nanofibrous chitosan membranes modified with polyethyleneimine for formaldehyde detection. Carbohydr. Polym. **108**(0), 192–199 (2014). doi:http://dx.doi.org/10.1016/j.carbpol.2014.02.088
104. X. Wang, B. Ding, J. Yu, J. Yang, Large-scale fabrication of two-dimensional spider-web-like gelatin nano-nets via electro-netting. Colloids Surf. B Biointerfaces **86**(2), 345–352 (2011). doi:http://dx.doi.org/10.1016/j.colsurfb.2011.04.018
105. D.C. Parajuli, M.P. Bajgai, J.A. Ko, H.K. Kang, M.S. Khil, H.Y. Kim, Synchronized polymerization and fabrication of poly(acrylic acid) and nylon hybrid mats in electrospinning. ACS Appl. Mater. Interfaces **1**(4), 750–757 (2009). doi:10.1021/am800191m
106. R. Nirmala, R. Navamathavan, M.H. El-Newehy, H.Y. Kim, Preparation and electrical characterization of polyamide-6/chitosan composite nanofibers via electrospinning. Mater. Lett. **65**(3), 493–496 (2011). doi:http://dx.doi.org/10.1016/j.matlet.2010.10.066
107. R. Nirmala, R. Navamathavan, H.-S. Kang, M.H. El-Newehy, H.Y. Kim, Preparation of polyamide-6/chitosan composite nanofibers by a single solvent system via electrospinning for biomedical applications. Colloids Surf. B Biointerfaces **83**(1), 173–178 (2011). doi:http://dx.doi.org/10.1016/j.colsurfb.2010.11.026
108. B. Ding, Y. Si, X. Wang, J. Yu, L. Feng, G. Sun, Label-free ultrasensitive colorimetric detection of copper(II) ions utilizing polyaniline/polyamide-6 nano-fiber/net sensor strips. J. Mater. Chem. **21**(35), 13345–13353 (2011). doi:10.1039/c1jm11851j
109. Y. Si, X. Wang, Y. Li, K. Chen, J. Wang, J. Yu, H. Wang, B. Ding, Optimized colorimetric sensor strip for mercury(ii) assay using hierarchical nanostructured conjugated polymers. J. Mater. Chem. A **2**(3), 645–652 (2014). doi:10.1039/c3ta13867d
110. Y. Li, Y. Si, X. Wang, B. Ding, G. Sun, G. Zheng, W. Luo, J. Yu, Colorimetric sensor strips for lead (II) assay utilizing nanogold probes immobilized polyamide-6/nitrocellulose nano-fibers/nets. Biosens. Bioelectron. **48**(0), 244–250 (2013). doi:http://dx.doi.org/10.1016/j.bios.2013.03.085
111. C.K. O'Sullivan, G.G. Guilbault, Commercial quartz crystal microbalances – theory and applications. Biosens. Bioelectron. **14**(8–9), 663–670 (1999). doi:http://dx.doi.org/10.1016/S0956-5663(99)00040-8

112. B. Ding, J.H. Kim, Y. Miyazaki, S.M. Shiratori, Electrospun nanofibrous membranes coated quartz crystal microbalance as gas sensor for NH3 detection. Sens Actuators B Chem. **101**(3), 373–380 (2004). doi:10.1016/j.snb.2004.04.008
113. B. Ding, M. Yamazaki, S. Shiratori, Electrospun fibrous polyacrylic acid membrane-based gas sensors. Sens Actuators B Chem. **106**(1), 477–483 (2005). doi:10.1016/j.snb.2004.09.010
114. S. Casilli, C. Malitesta, S. Conoci, S. Petralia, S. Sortino, L. Valli, Piezoelectric sensor functionalised by a self-assembled bipyridinium derivative: characterisation and preliminary applications in the detection of heavy metal ions. Biosens. Bioelectron. **20**(6), 1190–1195 (2004). doi:http://dx.doi.org/10.1016/j.bios.2004.04.028
115. A.J. Ricco, R.M. Crooks, G.C. Osbourn, Surface acoustic wave chemical sensor arrays: new chemically sensitive interfaces combined with novel cluster analysis to detect volatile organic compounds and mixtures. Acc. Chem. Res. **31**(5), 289–296 (1998). doi:10.1021/ar9600749
116. A. Palaniappan, X. Li, F.E.H. Tay, J. Li, X. Su, Cyclodextrin functionalized mesoporous silica films on quartz crystal microbalance for enhanced gas sensing. Sens. Actuators B **119** (1), 220–226 (2006). doi:http://dx.doi.org/10.1016/j.snb.2005.12.015
117. C. Zhang, X. Wang, J. Lin, B. Ding, J. Yu, N. Pan, Nanoporous polystyrene fibers functionalized by polyethyleneimine for enhanced formaldehyde sensing. Sens. Actuators B **152**(2), 316–323 (2011). doi:http://dx.doi.org/10.1016/j.snb.2010.12.028
118. Y.I. Korpan, M.V. Gonchar, A.A. Sibirny, C. Martelet, A.V. El'skaya, T.D. Gibson, A.P. Soldatkin, Development of highly selective and stable potentiometric sensors for formaldehyde determination. Biosens. Bioelectron. **15**(1–2), 77–83 (2000). doi:http://dx.doi.org/10.1016/S0956-5663(00)00054-3
119. R. Kataky, M.R. Bryce, L. Goldenberg, S. Hayes, A. Nowak, A biosensor for monitoring formaldehyde using a new lipophilic tetrathiafulvalene-tetracyanoquinodimethane salt and a polyurethane membrane. Talanta **56**(3), 451–458 (2002). doi:http://dx.doi.org/10.1016/S0039-9140(01)00567-7
120. X. Wang, F. Cui, J. Lin, B. Ding, J. Yu, S.S. Al-Deyab, Functionalized nanoporous TiO2 fibers on quartz crystal microbalance platform for formaldehyde sensor. Sens. Actuators B **171–172**, 658–665 (2012). doi:10.1016/j.snb.2012.05.050
121. P.-R. Chung, C.-T. Tzeng, M.-T. Ke, C.-Y. Lee, Formaldehyde gas sensors: a review. Sensors **13**(4), 4468–4484 (2013). doi:10.3390/s130404468
122. S. Srisuda, B. Virote, Adsorption of formaldehyde vapor by amine-functionalized mesoporous silica materials. J. Environ. Sci. **20**(3), 379–384 (2008). doi:http://dx.doi.org/10.1016/S1001-0742(08)60059-5
123. V.V. Sysoev, J. Goschnick, T. Schneider, E. Strelcov, A. Kolmakov, A gradient microarray electronic nose based on percolating SnO2 nanowire sensing elements. Nano Lett. **7**(10), 3182–3188 (2007)
124. J. Huang, Q. Wan, Gas sensors based on semiconducting metal oxide one-dimensional nanostructures. Sensors **9**(12), 9903–9924 (2009). doi:10.3390/s91209903
125. S. Bag, I.U. Arachchige, M.G. Kanatzidis, Aerogels from metal chalcogenides and their emerging unique properties. J. Mater. Chem. **18**(31), 3628–3632 (2008). doi:10.1039/B804011G
126. R. Liang, H. Cao, D. Qian, MoO3 nanowires as electrochemical pseudocapacitor materials. Chem. Commun. **47**(37), 10305–10307 (2011). doi:10.1039/C1CC14030B
127. M. Kimura, R. Sakai, S. Sato, T. Fukawa, T. Ikehara, R. Maeda, T. Mihara, Sensing of vaporous organic compounds by TiO_2 porous films covered with polythiophene layers. Adv. Funct. Mater. **22**(3), 469–476 (2012). doi:10.1002/adfm.201101953
128. A.W. Martinez, S.T. Phillips, M.J. Butte, G.M. Whitesides, Patterned paper as a platform for inexpensive, low-volume, portable bioassays. Angew. Chem. Int. Ed. **46**(8), 1318–1320 (2007). doi:10.1002/anie.200603817
129. A.W. Martinez, S.T. Phillips, G.M. Whitesides, E. Carrilho, Diagnostics for the developing world: microfluidic paper-based analytical devices. Anal. Chem. **82**(1), 3–10 (2009). doi:10.1021/ac9013989

130. W. Zhao, M.M. Ali, S.D. Aguirre, M.A. Brook, Y. Li, Paper-based bioassays using gold nanoparticle colorimetric probes. Anal. Chem. **80**(22), 8431–8437 (2008). doi:10.1021/ac801008q
131. R. Pelton, Bioactive paper provides a low-cost platform for diagnostics. TrAC Trends Anal. Chem. **28**(8), 925–942 (2009). doi:http://dx.doi.org/10.1016/j.trac.2009.05.005
132. X. Wang, Y. Si, X. Mao, Y. Li, J. Yu, H. Wang, B. Ding, Colorimetric sensor strips for formaldehyde assay utilizing fluoral-p decorated polyacrylonitrile nanofibrous membranes. Analyst **138**(17), 5129–5136 (2013). doi:10.1039/c3an00812f
133. S. Mukherjee, J.W. Yang, S. Hoffmann, B. List, Asymmetric enamine catalysis. Chem. Rev. **107**(12), 5471–5569 (2007). doi:10.1021/cr0684016
134. B.C. Ye, B.C. Yin, Highly sensitive detection of mercury(II) ions by fluorescence polarization enhanced by gold nanoparticles. Angew. Chem. Int. Ed. **47**(44), 8386–8389 (2008). doi:10.1002/anie.200803069
135. M. Zhang, L. Ge, S. Ge, M. Yan, J. Yu, J. Huang, S. Liu, Three-dimensional paper-based electrochemiluminescence device for simultaneous detection of Pb^{2+} and Hg^{2+} based on potential-control technique. Biosens. Bioelectron. **41**(0), 544–550 (2013). doi:http://dx.doi.org/10.1016/j.bios.2012.09.022
136. C.X. Tang, Y. Zhao, X.W. He, X.B. Yin, A "turn-on" electrochemiluminescent biosensor for detecting Hg2+ at femtomole level based on the intercalation of $Ru(phen)^{32+}$ into ds-DNA. Chem. Commun. **46**(47), 9022–9024 (2010). doi:10.1039/C0CC03495A
137. J. Liu, Y. Lu, Rational design of "turn-on" allosteric DNAzyme catalytic beacons for aqueous mercury ions with ultrahigh sensitivity and selectivity. Angew. Chem. Int. Ed. **46**(40), 7587–7590 (2007). doi:10.1002/anie.200702006
138. H.S. Kolla, S.P. Surwade, X. Zhang, A.G. MacDiarmid, S.K. Manohar, Absolute molecular weight of polyaniline. J. Am. Chem. Soc. **127**(48), 16770–16771 (2005). doi:10.1021/ja055327k
139. C. Alemán, C.A. Ferreira, J. Torras, A. Meneguzzi, M. Canales, M.A.S. Rodrigues, J. Casanovas, On the molecular properties of polyaniline: a comprehensive theoretical study. Polymer **49**(23), 5169–5176 (2008). doi:http://dx.doi.org/10.1016/j.polymer.2008.09.023
140. A. Varela-Álvarez, J.A. Sordo, G.E. Scuseria, Doping of polyaniline by acid – base chemistry: density functional calculations with periodic boundary conditions. J. Am. Chem. Soc. **127**(32), 11318–11327 (2005). doi:10.1021/ja051012t
141. D.P. Pompeani, M.B. Abbott, B.A. Steinman, D.J. Bain, Lake sediments record prehistoric lead pollution related to early copper production in North America. Environ. Sci. Technol. **47**(11), 5545–5552 (2013). doi:10.1021/es304499c
142. H. Cheng, Y. Hu, Lead (Pb) isotopic fingerprinting and its applications in lead pollution studies in China: a review. Environ. Pollut. **158**(5), 1134–1146 (2010). doi:http://dx.doi.org/10.1016/j.envpol.2009.12.028
143. G. Li, L. Zhang, Z. Li, W. Zhang, PAR immobilized colorimetric fiber for heavy metal ion detection and adsorption. J. Hazard. Mater. **177**(1–3), 983–989 (2010). doi:http://dx.doi.org/10.1016/j.jhazmat.2010.01.015
144. L. Fewtrell, World Health Organization, R. Kaufmann, A. Prüss-Üstün, World Health Organization Protection of the Human Environment, *Lead: Assessing the Environmental Burden of Disease at National and Local Levels* (World Health Organization, Protection of the Human Environment, 2003), http://www.who.int/quantifying_ehimpacts/publications/en/leadebd2.pdf
145. M.G. Aylmore, Treatment of a refractory gold-copper sulfide concentrate by copper ammoniacal thiosulfate leaching. Miner. Eng. **14**(6), 615–637 (2001). doi:http://dx.doi.org/10.1016/S0892-6875(01)00057-7
146. G.H. Liu, J.Y. Yang, Content-based image retrieval using color difference histogram. Pattern Recogn. **46**(1), 188–198 (2013). doi:http://dx.doi.org/10.1016/j.patcog.2012.06.001
147. M.M. Hawkeye, M.J. Brett, Optimized colorimetric photonic-crystal humidity sensor fabricated using glancing angle deposition. Adv. Funct. Mater. **21**(19), 3652–3658 (2011). doi:10.1002/adfm.201100893